

Radial Neighbors for Provably Accurate Scalable Approximations of Gaussian Processes

BY YICHEN ZHU

Bocconi Institute for Data Science and Analytics, Bocconi University, Milan, MI, Italy.
 yichen.zhu@unibocconi.it

MICHELE PERUZZI

Department of Biostatistics, University of Michigan, Ann Arbor, Michigan, U.S.A.
 peruzzi@umich.edu

CHENG LI

Department of Statistics and Data Science, National University of Singapore, Singapore.
 stalic@nus.edu.sg

AND DAVID B. DUNSON

Department of Statistical Science & Mathematics, Duke University, North Carolina, U.S.A.
 dunson@duke.edu

SUMMARY

In geostatistical problems with massive sample size, Gaussian processes can be approximated using sparse directed acyclic graphs to achieve scalable $O(n)$ computational complexity. In these models, data at each location are typically assumed conditionally dependent on a small set of parents which usually include a subset of the nearest neighbors. These methodologies often exhibit excellent empirical performance, but the lack of theoretical validation leads to unclear guidance in specifying the underlying graphical model and sensitivity to graph choice. We address these issues by introducing radial neighbors Gaussian processes (RadGP), a class of Gaussian processes based on directed acyclic graphs in which directed edges connect every location to all of its neighbors within a predetermined radius. We prove that any radial neighbors Gaussian process can accurately approximate the corresponding unrestricted Gaussian process in Wasserstein-2 distance, with an error rate determined by the approximation radius, the spatial covariance function, and the spatial dispersion of samples. We offer further empirical validation of our approach via applications on simulated and real world data showing excellent performance in both prior and posterior approximations to the original Gaussian process.

Some key words: Approximations; Directed acyclic graph; Gaussian process; Spatial statistics; Wasserstein distance.

1. INTRODUCTION

Data indexed by spatial coordinates are routinely collected in massive quantities due to the rapid pace of technological development in imaging sensors, wearables and tracking devices. Statistical models of spatially correlated data are most commonly built using Gaussian processes due to their flexibility and their ability to straightforwardly quantify uncertainty. Spatial depen-

dence in the data is typically characterized by a parametric covariance function whose unknown parameters are estimated by repeatedly evaluating a multivariate normal density with a dense covariance matrix. At each density evaluation, the inverse covariance matrix and its determinant must be computed at a complexity that is cubic on the data dimension n . This steep cost severely restricts the applicability of Gaussian processes on modern geolocated datasets. This problem is exacerbated in Bayesian hierarchical models computed via Markov-chain Monte Carlo (MCMC) because several thousands of $O(n^3)$ operations must be performed to fully characterize the joint posterior distribution.

A natural idea for retaining the flexibility of Gaussian processes while circumventing their computational bottlenecks is to use approximate methods for evaluating high dimensional multivariate Gaussian densities. If the scalable approximation is “good” in some sense, then one can use the approximate method for backing out inferences on the original process parameters. A multitude of such scalable methods has been proposed in the literature. Low-rank methods using inducing variables or knots (Quiñero-Candela & Rasmussen, 2005; Cressie & Johannesson, 2008; Banerjee et al., 2008; Finley et al., 2009; Guhaniyogi et al., 2011; Sang et al., 2011) are only appropriate for approximating very smooth Gaussian processes because the number of inducing variables must increase polynomially fast with the sample size to avoid oversmoothing of the spatial surface (Stein, 2014; Burt et al., 2020). Scalability can also be achieved by assuming sparsity of the Gaussian covariance matrix via compactly supported covariance functions (Furrer et al., 2006; Kaufman et al., 2008; Bevilacqua et al., 2019); these methods operate by assuming marginal independence of pairs of data points that are beyond a certain distance from each other. See also the related method of Gramacy & Apley (2015). Using a similar intuition, one can achieve scalability by approximating the high dimensional Gaussian density with a product of small dimensional densities that characterize dependence of nearby data points. Composite likelihood methods (Bai et al., 2012; Eidsvik et al., 2014; Bevilacqua & Gaetan, 2015) approximate the high dimensional Gaussian density with the product of sub-likelihoods, whereas Gaussian Markov Random Fields (GMRF; Cressie, 1993; Rue & Held, 2005) approximate it via a product of conditional densities whose conditioning sets include all the local spatial neighbors.

Markovian conditional independence assumptions based on spatial neighborhoods can be visualized as a sparse undirected graphical model; these assumptions are intuitively appealing and lead to sparse precision matrices and more efficient computations (Rue, 2001). However, the normalizing constant of GMRF densities may require additional expensive computations, and additional approximation steps may be required when making predictions at new spatial locations because GMRFs do not necessarily extend to a standalone stochastic process. Both these problems can be resolved by ordering the data and conditioning only using previously ordered data points. Because one can now use a directed acyclic graph to represent conditional independence in the data, this approximation (due to Vecchia, 1988) immediately leads to a valid density which can be extended to a standalone stochastic process.

There is a rich literature on approximations of Gaussian processes using directed acyclic graphs. In addition to extensions of Vecchia’s method (Datta et al., 2016; Finley et al., 2019; Katzfuss & Guinness, 2021), scalable models can be built on domain partitions (Peruzzi et al., 2022), and generalizations are available for non-Gaussian and multivariate data (Zilber & Katzfuss, 2021; Peruzzi & Dunson, 2022, 2024) as well as for modeling nonstationary processes (Jin et al., 2021; Kidd & Katzfuss, 2022). However, we identify two issues with current approaches based on Vecchia’s approximation. First, because the graphical model representation of Vecchia approximations is not unique, the numerical performance of these methods can be sensitive to the choice of graphical model in certain scenarios (Guinness, 2018). There is no consensus on how to choose these conditioning sets. Second, although their performance has been demonstrated in

practice (Heaton et al., 2019) and some theory on parameter estimation is available (Zhang, 2012; Zhang et al., 2023), there is limited theoretical study focused on accuracy of the approximation. The recent work by Schäfer et al. (2021) established Kullback-Leibler divergence bounds for Vecchia approximations, but under strong conditions that are difficult to verify for commonly used spatial covariance functions.

In this paper, we address these two issues by introducing a novel method and corresponding theoretical guarantees. Our radial neighbors Gaussian processes scalably approximate an initial Gaussian process by assuming conditional independence at spatial locations as prescribed by a directed acyclic graph. For every location in the graph, directed edges connect it to all of its neighbors within a predetermined radius ρ .

We also introduce—to the best of our knowledge—the first general theoretical result regarding the closeness between a Vecchia-like method and the Gaussian process it approximates. We show that any process from the RadGP family can accurately approximate the original Gaussian processes in Wasserstein-2 distance, with an error rate determined by the approximation radius, the spatial covariance function, and the spatial dispersion of samples. This approximation accuracy is insensitive to the graphical structure as long as the graphical structure does not alter the radial condition of RadGP. Our theory can be applied to a wide range of covariance functions including the Matérn, Gaussian and generalized Cauchy models. Empirical studies demonstrate that our RadGPs have excellent performance in approximating a Gaussian process prior and the posterior from a Gaussian process regression model.

2. RADIAL NEIGHBORS GAUSSIAN PROCESS

2.1. Radial Neighbors Graphs

Let the spatial domain Ω be a connected subset of \mathbb{R}^d . Let $Z = (Z_s : s \in \Omega)$ be a real valued Gaussian process on $\Omega \subset \mathbb{R}^d$ with zero mean and covariance function $K : \Omega \times \Omega \rightarrow \mathbb{R}$ such that for all $s_1, s_2 \in \Omega$, $\mathbb{E}(Z_{s_1}) = 0$ and $\text{Cov}(Z_{s_1}, Z_{s_2}) = K(s_1, s_2)$. The objective of this paper is to approximate the process Z with another process \hat{Z} such that the distance between \hat{Z} and Z is small in some metric and finite marginal densities of \hat{Z} are easy to compute.

Let $\mathcal{D} = \{w_1, w_2, \dots, w_n\}$ be a finite collection of locations in Ω . A ρ -radial neighbors graph on \mathcal{D} is defined to be a directed acyclic graph such that for any $w_i, w_j \in \mathcal{D}$ with $\|w_i - w_j\|_2 < \rho$, there is a directed edge between w_i and w_j . Such radial neighbors graphs are not unique. Section 2.2 provides one practical way of constructing a radial neighbors graph that will be used in our experimental studies, while Section 2.3 presents how to build a Gaussian process from any radial neighbors graph. Our theory in Section 3 applies to any Gaussian process built from a radial neighbors graph, not just the specific graph we constructed in Section 2.2.

2.2. Construction of a Radial Neighbors Graph

We present a procedure to construct the radial neighbors graph that will be used for experiments in Section 5. First, we specify an order of all locations in \mathcal{D} . This is done by choosing a “center” location of \mathcal{D} and sorting all the locations in \mathcal{D} according to their distances to this “center” in a non-decreasing order. If the locations in \mathcal{D} are roughly evenly distributed in the domain Ω , then the coordinates of this center are set as the arithmetic mean of the coordinates of all locations in \mathcal{D} .

Next, once an order of locations in \mathcal{D} is obtained, for each location $w_i \in \mathcal{D}$, we set the parent set of w_i to be all the locations preceding w_i in this order and within ρ distance to w_i . As a consequence, for all locations within ρ radius of w_i , the ones that precede it are its parents, whereas the ones that follow it are its children. This construction satisfies the definition of radial

neighbors graphs in Section 2.1 that any pair of locations (w_i, w_j) with $\|w_i - w_j\|_2 < \rho$ have a directed edge connecting them.

Depending on the spatial dispersion of locations in \mathcal{D} , some locations may not have neighbors within ρ distance. We thus populate the parent set of a location $w_i \in \mathcal{D}$ without ρ -neighbors by drawing an edge from w_i 's nearest neighbor among all locations that precede w_i in the order. This step ensures that the resulting directed acyclic graph is connected.

If the locations in \mathcal{D} are roughly evenly distributed in the domain Ω , once the first i locations are chosen and the directed graph on them is constructed, our procedure roughly chooses the $(i + 1)$ th location to be as close to the first i locations as possible. Since spatial covariance function $K(s_1, s_2)$ is often relatively large when s_1 and s_2 are close to each other, our procedure aims to minimize the conditional variance of the $(i + 1)$ th location given the first i locations, or in other words, maximize the spatial information that the $(i + 1)$ th location can borrow from the first i locations. Figure 1 illustrates the process of building this radial neighbors graph when \mathcal{D} is a 15×15 grid on $[0, 1]^2$.

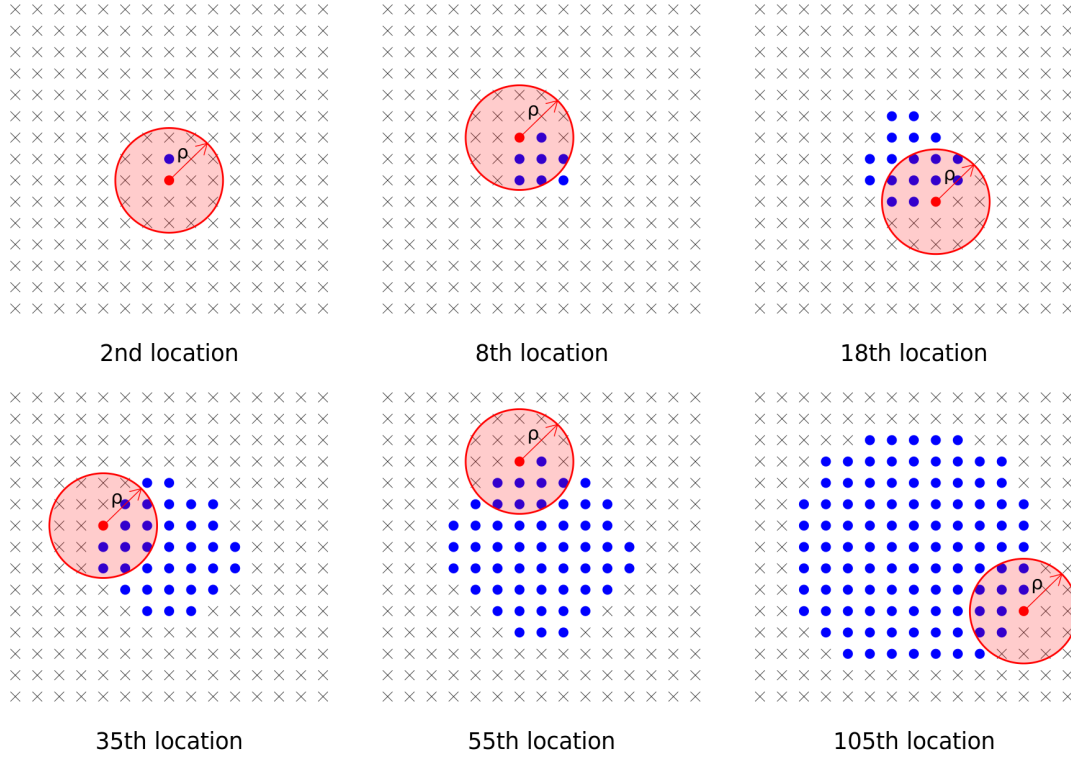


Fig. 1: Construction of a radial neighbors graph. In each subpanel, the location in red follows all locations in blue and precedes all locations in gray in the predetermined order. The parent set for the location in red is built by drawing a directed edge to it from each blue location inside the red circle.

Finally, if we have a new data set $\tilde{\mathcal{D}}$, the radial neighbors graph constructed on \mathcal{D} can be extended to a radial neighbors graph on $\mathcal{D} \cup \tilde{\mathcal{D}}$. Specifically, once an ordering of locations in $\tilde{\mathcal{D}}$ is obtained, we concatenate the ordering of locations in \mathcal{D} and $\tilde{\mathcal{D}}$ to obtain an ordering of locations $\mathcal{D} \cup \tilde{\mathcal{D}}$. We then construct a radial neighbors graph on $\mathcal{D} \cup \tilde{\mathcal{D}}$ via the same procedure

as described above. The final graph will contain the graph on \mathcal{D} as a subgraph. This extension framework will be useful when extending a graph from training data to test data.

For some dataset, the spatial dispersion of both training and testing locations can be highly uneven. While a radial neighbor graph ensures all locations are connected in the same directed graph, it can still result in poor predictions on some test locations. We can mitigate this issue by artificially adding more test locations, so that each test locations receives a decent number of parents.

2.3. Gaussian Processes from Radial Neighbors Graphs

Given a ρ -radial neighbors graph on $\mathcal{D} = \{w_1, w_2, \dots, w_n\}$ defined in Section 2.1, we can build a RadGP on \mathcal{D} in which each w_i is conditionally only dependent on its parent set. Let the symbol $\stackrel{d}{=}$ denote equality in distribution and define $\Sigma_{A,B}$ as the covariance matrix between two spatial location sets A and B under the covariance function $K(\cdot, \cdot)$. The conditional distribution of \hat{Z}_{w_i} is defined as

$$[\hat{Z}_{w_i} \mid \hat{Z}_{w_j}, j < i] \stackrel{d}{=} [\hat{Z}_{w_i} \mid \hat{Z}_{\text{pa}(w_i)}] \stackrel{d}{=} [Z_{w_i} \mid Z_{\text{pa}(w_i)}] \\ \sim N\left(\Sigma_{\text{pa}(w_i), w_i}^T \Sigma_{\text{pa}(w_i), \text{pa}(w_i)}^{-1} \hat{Z}_{\text{pa}(w_i)}, K(w_i, w_i) - \Sigma_{\text{pa}(w_i), w_i}^T \Sigma_{\text{pa}(w_i), \text{pa}(w_i)}^{-1} \Sigma_{\text{pa}(w_i), w_i}\right), \quad (1)$$

where for $i = 1$ the parent set $\text{pa}(w_1)$ is empty.

Equation (1) defines the distribution of \hat{Z} on all finite subsets of \mathcal{D} , which essentially says the conditional distribution of \hat{Z}_{w_i} given the process \hat{Z} on all locations preceding w_i has the same law as the conditional distribution of Z_{w_i} given the process Z on the parent set $\text{pa}(w_i)$. We then extend this process \hat{Z} to arbitrary finite subsets of the whole space Ω . For all $s \in \Omega \setminus \mathcal{D}$, we define the parents of s as $\text{pa}(s) = \{s' \in \mathcal{D} : \|s' - s\|_2 < \rho\}$. For any finite set $U \subset \Omega \setminus \mathcal{D}$, we define the conditional distribution of \hat{Z}_U given $\hat{Z}_{\mathcal{T}_1}$ as

$$p(\hat{Z}_U \mid \hat{Z}_{\mathcal{D}}) = \prod_{s \in U} p(\hat{Z}_s \mid \hat{Z}_{\text{pa}(s)}) = \prod_{s \in U} p(Z_s \mid Z_{\text{pa}(s)}), \\ [\hat{Z}_s \mid \hat{Z}_{\text{pa}(s)}] \sim N\left(\Sigma_{\text{pa}(s), s}^T \Sigma_{\text{pa}(s), \text{pa}(s)}^{-1} \hat{Z}_{\text{pa}(s)}, K(s, s) - \Sigma_{\text{pa}(s), s}^T \Sigma_{\text{pa}(s), \text{pa}(s)}^{-1} \Sigma_{\text{pa}(s), s}\right). \quad (2)$$

Equations (1) and (2) together give the joint distribution of \hat{Z} on any finite subset of Ω . Specifically, for a generic finite set $A = U \cup V$ with $U \subset \Omega \setminus \mathcal{D}$ and $V \subset \mathcal{D}$, the joint density of \hat{Z} on A implied by Equations (1) and (2) is

$$p(\hat{Z}_A) = p(\hat{Z}_U \mid \hat{Z}_{\mathcal{D}}) \int \prod_{i=1}^n p(\hat{Z}_{w_i} \mid \hat{Z}_{\text{pa}(w_i)}) \prod_{w_i \in \mathcal{D} \setminus V} dw_i. \quad (3)$$

Equations (1)-(3) complete the definition of our RadGP.

LEMMA 1. *The radial neighbors Gaussian process (RadGP) $\hat{Z}(\cdot)$ is a valid Gaussian process on the whole spatial domain Ω .*

The proof of Lemma 1 relies on the Kolmogorov extension theorem and is available at Section S1 of the Supplementary Material.

3. THEORETICAL PROPERTIES

3.1. Wasserstein Distance Between Gaussian Processes

The objective of this section is to establish theoretical upper bounds for the Wasserstein distance between the original Gaussian process and any RadGP on \mathcal{D} described above. For two

generic random vectors Z_1, Z_2 defined on the same space \mathcal{Z} following the probability distributions μ_1, μ_2 , their Wasserstein-2 (W_2) distance is

$$W_2(Z_1, Z_2) = \left\{ \min_{\tilde{\mu} \in \mathcal{M}} \int_{\mathcal{Z} \times \mathcal{Z}} \|z_1 - z_2\|_2^2 d\tilde{\mu}(z_1, z_2) \right\}^{1/2},$$

where \mathcal{M} is the set of all probability distributions on the product space $\mathcal{Z} \times \mathcal{Z}$ whose marginals are μ_1 and μ_2 . Let $Z_{\mathcal{D}}$ and $\hat{Z}_{\mathcal{D}}$ be the random vectors from the original Gaussian process and the RadGP on the set \mathcal{D} . Denote the covariance matrix of $Z_{\mathcal{D}}$ and $\hat{Z}_{\mathcal{D}}$ as $\Sigma_{\mathcal{D}\mathcal{D}}$ and $\hat{\Sigma}_{\mathcal{D}\mathcal{D}}$, respectively. Then the Wasserstein-2 distance between $Z_{\mathcal{D}}$ and $\hat{Z}_{\mathcal{D}}$ has a closed form (Gelbrich, 1990):

$$W_2^2(Z_{\mathcal{D}}, \hat{Z}_{\mathcal{D}}) = \text{tr}(\Sigma_{\mathcal{D}\mathcal{D}}) + \text{tr}(\hat{\Sigma}_{\mathcal{D}\mathcal{D}}) - 2\text{tr}\{(\Sigma_{\mathcal{D}\mathcal{D}}^{1/2} \hat{\Sigma}_{\mathcal{D}\mathcal{D}} \Sigma_{\mathcal{D}\mathcal{D}}^{1/2})^{1/2}\}, \quad (4)$$

where $\text{tr}(A)$ denotes the trace of a square matrix A . The right-hand side of equation (4) involves various matrix powers that are difficult to analyze. Fortunately, for Gaussian measures, the squared Wasserstein-2 distance can be upper bounded by the trace norm of the difference between their covariance matrices, which greatly simplifies our analysis.

3.2. Spatial Decaying Families

We consider the Gaussian process $Z = (Z_s : s \in \Omega)$ with zero mean and an isotropic nonnegative covariance function $K(\cdot, \cdot)$. Thus we can reformulate K as $K(s_1, s_2) = K_0(\|s_1 - s_2\|_2)$ for all $s_1, s_2 \in \Omega$, where $K_0 : [0, +\infty) \rightarrow [0, +\infty)$. For all $r > 0$, define the function $v_r(\cdot) : \mathbb{R} \rightarrow \mathbb{R}_+$ as $v_r(x) = \sum_{k=0}^{+\infty} |x|^k / (k!)^r$. Then $1/v_r(x)$ is a monotone decreasing function of x , where a larger r results in a slower decay rate in $1/v_r(x)$. Specifically, $1/v_1(x) = \exp(-x)$ and $1/v_r(x)$ with $r > 1$ has a decay rate faster than all polynomials but slower than the exponential function. We also define a series of polynomials $c_r(x) = 1 + x^r$ for $r > 0$. For each v_r with $r > 1$ and each c_r with $r > 0$, we define the following families of Gaussian processes:

$$\mathcal{Z}_{v_r} = \left\{ Z = (Z_s : s \in \Omega) : K_0(\|s_1 - s_2\|_2) \leq \frac{1}{v_r(\|s_1 - s_2\|_2)(1 + \|s_1 - s_2\|_2^{d+1})} \right\}, \quad (5)$$

$$\mathcal{Z}_{c_r} = \left\{ Z = (Z_s : s \in \Omega) : K_0(\|s_1 - s_2\|_2) \leq \frac{1}{(1 + \|s_1 - s_2\|_2)^r} \right\}. \quad (6)$$

Intuitively, \mathcal{Z}_{v_r} is the family of isotropic Gaussian processes whose covariance function decays no slower than some subexponential rate of the spatial distance, while \mathcal{Z}_{c_r} is the family with covariance functions decaying no slower than an r th order polynomial of the spatial distance.

The objective of our theoretical study is to bound the Wasserstein-2 distance between the marginal distribution of RadGP and original Gaussian process on \mathcal{D} when the original process belongs to the two spatial decaying families in (5) and (6):

$$\sup_{Z \in \mathcal{Z}_{v_r}} W_2^2(Z_{\mathcal{D}}, \hat{Z}_{\mathcal{D}}) \quad \text{and} \quad \sup_{Z \in \mathcal{Z}_{c_r}} W_2^2(Z_{\mathcal{D}}, \hat{Z}_{\mathcal{D}}). \quad (7)$$

3.3. Rate of Approximation

For the finite set \mathcal{D} described above, we define the minimal separation distance among all spatial locations in \mathcal{D} as $q = \min_{1 \leq i < j \leq |\mathcal{D}|} \|w_i - w_j\|_2$. This minimal separation distance is a parsimonious statistic for describing the spatial dispersion of \mathcal{D} , and is useful in bounding various quantities such as the maximal eigenvalue and condition number of $\Sigma_{\mathcal{D}\mathcal{D}}$; see Lemma S2 of the Supplementary Material for details. Let $\hat{K}_0(w) = (2\pi)^{-d/2} \int K_0(x) \exp(-\imath w^T x) dx$ be the Fourier transform of K_0 where $\imath^2 = -1$, and let $\phi_0(x) = \inf_{\|w\|_2 \leq 2x} \hat{K}_0(w)$ for all $x > 0$. For two positive sequences a_n and b_n , we use $a_n \lesssim b_n$ to denote the relation that $a_n \leq C b_n$ for

all n and some finite constant C . We have the following theorems on the Wasserstein-2 distance between the RadGP and the original Gaussian process. The constants c_1, c_2 are from Lemma S2 while c_3 is from the proof of Lemma S5 in the Supplementary Material, all of which only depend on the dimension d of the spatial domain Ω .

THEOREM 1. *For all radial neighbors Gaussian processes \hat{Z} , for the family \mathcal{Z}_{v_r} in (5) with $r > 1$, if $0 < q < 1$ and $n^{1/2}\{v_r(\rho d^{-1/2})\}^{-1}\{\phi_0(c_2/q)\}^{-9/2}v_{r-1}[c_3\{\phi_0(c_2/q)\}^{-1}] \leq c_6$ hold for some constant c_6 only dependent on d , then*

$$\sup_{Z \in \mathcal{Z}_{v_r}} W_2^2(Z_{\mathcal{D}}, \hat{Z}_{\mathcal{D}}) \lesssim \frac{n}{v_r(\rho d^{-1/2})} \{\phi_0(c_2/q)\}^{-5} q^{-d} v_{r-1} [c_3 \{\phi_0(c_2/q)\}^{-1}]. \quad (8)$$

Else if $q \geq 1$ and $n^{1/2}/v_r(\rho d^{-1/2}) \leq c'_6$ hold for some constant c'_6 only dependent on d , then $\sup_{Z \in \mathcal{Z}_{v_r}} W_2^2(Z_{\mathcal{D}}, \hat{Z}_{\mathcal{D}}) \lesssim n/v_r(\rho d^{-1/2})$.

THEOREM 2. *For all radial neighbors Gaussian processes \hat{Z} , for the family \mathcal{Z}_{c_r} in (6) with $r \geq d + 1$, if $0 < q < 1$ and $n^{1/2}(1 + \rho d^{-1/2})^{-(r-d-1)} q^{(r-7)d} \{\phi_0(c_2/q)\}^{-(r+4)} (c_1 c_5 d 2^{d-1} \pi / \sqrt{6})^r \leq c_7$ hold for some constant c_7 only dependent on d , then*

$$\sup_{Z \in \mathcal{Z}_{c_r}} W_2^2(Z_{\mathcal{D}}, \hat{Z}_{\mathcal{D}}) \lesssim \frac{n}{(1 + \rho d^{-1/2})^{r-d-1}} q^{(r-8)d} \{\phi_0(c_2/q)\}^{-(r+9/2)} (c_1 c_5 d 2^{d-1} \pi / \sqrt{6})^r, \quad (9)$$

Else if $q \geq 1$ and $n^{1/2}(1 + \rho d^{-1/2})^{-(r-d-1)} \{\phi_0(c_2/q)\}^{-r} (c_1 c_5 d 2^{d-1} \pi / \sqrt{6})^r \leq c'_7$ hold for some constant c'_7 only dependent on d , then $\sup_{Z \in \mathcal{Z}_{c_r}} W_2^2(Z_{\mathcal{D}}, \hat{Z}_{\mathcal{D}}) \lesssim n(1 + \rho d^{-1/2})^{-(r-d-1)}$.

The conditions for the above theorems, namely the equations regarding c_6, c'_6, c_7, c'_7 , are necessary but not sufficient conditions for the upper bounds of Wasserstein-2 distance to go to zero. Thus, they can be safely ignored if we aim for accurate approximations. We now give a detailed analysis of these upper bounds for Wasserstein-2 distance involving three variables: the sample size n , the minimal separation distance q , and the approximation radius ρ in the RadGP. We will discuss from the perspectives of both finite samples and asymptotics. From a finite sample perspective, we fix two out of three variables and discuss how and why the upper bounds change as the remaining variable changes; from an asymptotic perspective, we describe the relations between n, q and ρ such that as n goes to infinity, the Wasserstein-2 distance goes to zero.

Viewing Theorems 1 and 2 as finite sample bounds, the upper bounds are linearly dependent on the sample size n . This directly follows from the definition of Wasserstein distance which measures the difference between two n -dimensional Gaussian distributions. Provided both the minimal separation distance q and approximation radius ρ are fixed, as the sample size n increases, the local structure for existing locations will not change and the approximation accuracy for them will not improve. Thus, adding more locations will lead to a linearly increasing approximation error in the squared W_2 distance.

Second, the upper bounds on the squared W_2 distance decay with respect to the approximation radius $\rho d^{-1/2}$ at the same rate as the spatial covariance function with respect to the spatial distance, up to a $(d + 1)$ th order polynomial. For Theorem 1, the covariance function is required to decay faster than $1/v_r(x)$ by a polynomial $1 + x^{d+1}$ as defined in equation (5); for Theorem 2, the covariance function decays faster than an r th order polynomial while the upper bound of W_2 distance decays at an $(r - d - 1)$ th order polynomial. The difference between the decay rate of the covariance function and the W_2 distance in Theorems 1 and 2 comes from the fact that high dimension reduces the effective decay rate of covariance function. For example, under a fixed minimal separation distance, when $d = 1$, as long as the covariance function decays faster than $1/x$ by a polynomial term, the matrix $\Sigma_{\mathcal{D}\mathcal{D}}$ has a bounded l_1 norm regardless of sample size; however, for a general d dimensional space, the covariance function must decay faster than $1/x^d$

for $\Sigma_{\mathcal{D}\mathcal{D}}$ to have a bounded l_1 norm. These upper bounds show that the approximation radius ρ indeed controls the approximation accuracy. Specifically, for fixed q and n , we can reach an arbitrarily small W_2 error by increasing ρ over some threshold value; see our detailed conditions on ρ in Corollary 1 for various types of covariance functions.

Third, for fixed ρ and n , both upper bounds in the two theorems increase as the minimal separation distance q decreases. This is because as the minimal separation distance decreases, spatial locations get closer to each other and the covariance matrix gets close to singular, leading to a larger approximation error.

From the asymptotic perspective, we can increase the sample size n while viewing the minimal separation distance q and the approximation radius ρ as some functions of n . The objective is to choose an approximation radius ρ dependent on n and q such that the squared Wasserstein distance goes to zero as n goes to infinity. We first present a corollary showing how to choose such ρ for three commonly used covariance functions, where the convergence is understood in the sense that q is also a function of n .

COROLLARY 1. *We have $W_2^2(Z_{\mathcal{D}}, \hat{Z}_{\mathcal{D}}) \rightarrow 0$ as $n \rightarrow \infty$ if one of the following conditions is satisfied:*

(1) *The covariance function is the isotropic Matérn: $K_0(s_1 - s_2) = \tau^2 2^{1-\nu} \Gamma(\nu)^{-1} (\phi \|s_1 - s_2\|)^\nu \mathcal{K}_\nu(\phi \|s_1 - s_2\|_2)$ with $q < 1/\phi$. Define the constant $c_{m,1} = \Gamma(\nu) / \{\tau^2 2^d \pi^{d/2} \Gamma(\nu + d/2)\}$. The approximation radius ρ satisfies*

$$\rho \geq \frac{d^{1/2}}{\phi} \left[c_3 c_{m,1} \left(1 + \frac{4c_2^2}{\phi^2 q^2} \right)^{\nu + \frac{d}{2}} + \ln \left\{ c_{m,1} n q^{-d} \left(1 + \frac{4c_2^2}{\phi^2 q^2} \right)^{5(\nu + \frac{d}{2})} \right\} \right]^3.$$

(2) *The covariance function is Gaussian $K_0(\|s_1 - s_2\|_2) = \tau^2 \exp(-a \|s_1 - s_2\|_2^2)$ with $q < a^{-1/2}$. The approximation radius ρ satisfies*

$$\rho \geq \left(\frac{d}{a} \right)^{1/2} \left[c_3 \tau^{-2} \exp \{ c_2^2 / (a q^2) \} + \ln(n q^{-d} \tau^{-10}) + \frac{5c_2^2}{a q^2} \right]^3.$$

(3) *The covariance function is the generalized Cauchy $K_0(\|s_1 - s_2\|_2) = \tau^2 \{ 1 + (\phi \|s_1 - s_2\|)^\delta \}^{-\lambda/\delta}$ with parameter $\lambda > d + 1$ and $q < \phi$. Let c_9 be a constant dependent on dimension d and covariance function parameters $\tau^2, \phi, \delta, \lambda$. The approximation radius ρ satisfies*

$$\rho \geq c_9 q^{-\frac{\frac{25}{2}d + \delta(\lambda + \frac{9}{2})}{\lambda - (d+1)}} n^{\frac{1}{\lambda - (d+1)}}.$$

We then analyze our main theorems from the asymptotic perspective and verify the analysis using the three examples in Corollary 1. Depending on whether and how the minimal separation distance q changes with respect to the sample size n , there are three commonly used asymptotic frameworks: fixed domain, mixed domain and increasing domain asymptotics.

Under the increasing domain setting, as n goes to infinity, the radius of the domain Ω increases while the minimal separation distance q is fixed. Therefore, as long as $n \gtrsim d^{1/2} v_r^{-1}(n)$ under conditions of Theorem 1 or $n \gtrsim d^{1/2} n^{1/(r-d-1)}$ under conditions of Theorem 2, we have $o(1)$ approximation error. When applied to Matérn covariance in case (1) and Gaussian covariance in case (2) of Corollary 1, this yields a slowly increasing rate of $O(\ln^3 n)$ for the approximation radius ρ , which is much smaller than the sample size n . On the other hand, when the covariance function decays polynomially such as the generalized Cauchy in case (3) of Corollary 1, the approximation radius ρ needs to increase at a polynomial rate of sample size n . This is because for covariance functions that decrease slowly in the spatial distance, one needs more spatial locations and a larger approximation radius to capture the dependence information.

Under the mixed domain setting, as n goes to infinity, the radius of the domain Ω increases with n while the minimal separation distance q also decreases with n . By solving the inequalities on the right hand side of equations (8) and (9) being no greater than $o(1)$, we obtain the lower bound of ρ that guarantees the $o(1)$ approximation error. Corollary 1 directly shows such lower bounds for Matérn, Gaussian and generalized Cauchy covariance functions. We can still achieve the $o(1)$ approximation error as long as these lower bounds of ρ in the three cases of Corollary 1 increase slower than the radius of the domain Ω . Otherwise, if ρ increases exactly at the same rate as the radius of Ω , RadGP is identical to the original Gaussian process and does not make any approximation at all. Our theory is not applicable when the lower bounds of ρ exceed the radius of domain Ω . In particular, for the fixed domain setting, the radius of Ω is fixed as a constant and the minimal separation distance q decreases to zero at a rate no slower than $O(n^{-1/d})$. In such case, the lower bounds of ρ in Corollary 1 will diverge with n , and therefore Theorems 1 and 2 do not provide a vanishing bound for Wasserstein-2 distances.

Our results fill a major gap in the literature by providing the previously lacking theoretical support for popular local or neighborhood-based Gaussian process approximations. Our theory only requires knowledge of the spatial decaying pattern of the covariance functions (e.g., exponential and polynomial in \mathcal{L}_{v_r} and \mathcal{L}_{c_r} , respectively). These conditions are easily verifiable, with derivations for the Matérn, Gaussian and the generalized Cauchy covariance functions provided in Corollary 1. Similar techniques can be used for a wider range of stationary covariance functions. Furthermore, our novel theory explicitly links the approximation quality from choosing radius ρ with the minimal separation distance q and the sample size n , both of which are readily available from observed data.

4. BAYESIAN REGRESSION WITH RADGP

Consider a linear regression model with spatial latent effects as:

$$Y(s) = X(s)\beta + Z(s) + \epsilon(s), \quad s \in \Omega, \quad (10)$$

where $X(s)$ are covariates at location s , β are regression coefficients for the covariates, $Z(s)$ is a Gaussian process with zero mean and covariance function $K_\theta : \Omega \times \Omega \rightarrow \mathbb{R}$, and $\epsilon(s)$ is a white noise process. Researchers observe $Y(s)$, $X(s)$ at a collection of training locations \mathcal{T}_1 with the objective of estimating the regression coefficients β , the covariance function parameters θ , and the spatial random effects $Z(s)$ at both training locations \mathcal{T}_1 and test locations $\mathcal{T}_2 \subset \Omega$. If the spatial random effects $Z(s)$ are not of interest, one can combine $Z(s)$ and $\epsilon(s)$ into one Gaussian process, known as the response model. This is described in Section S4.2 of the Supplementary Material. Hereafter we assume that inference on $Z(s)$ is desired. Let $Z_{\mathcal{T}_1}$ denote the column vector consisting of $(Z(s) : s \in \mathcal{T}_1)$. Similarly define other notations with \mathcal{T}_i as subscripts. Endow the spatial random effects on $\mathcal{T}_1 \cup \mathcal{T}_2$ with our RadGP prior defined in Section 2.3, which is built on the radial neighbors graph constructed in Section 2.2 such that the locations in the training set \mathcal{T}_1 precede locations in the test set \mathcal{T}_2 . The full Bayesian model can be outlined as follows:

$$\begin{aligned} (\beta, \theta, \sigma^2) &\sim p(\beta)p(\theta)p(\sigma^2), \quad \epsilon(s) \stackrel{\text{i.i.d.}}{\sim} N(0, \sigma^2), s \in \Omega, \quad \hat{Z}_{\mathcal{T}_1} | \theta \sim \prod_{s \in \mathcal{T}_1} p(\hat{Z}_s | \hat{Z}_{\text{pa}(s)}), \\ p(\hat{Z}_{\mathcal{T}_2} | \hat{Z}_{\mathcal{T}_1}, \theta) &\propto \prod_{s \in \mathcal{T}_2} p(\hat{Z}_s | \hat{Z}_{\text{pa}(s)}), \quad Y(s) = X(s)\beta + \hat{Z}(s) + \epsilon(s), \quad \text{for } s \in \Omega. \end{aligned} \quad (11)$$

The priors for β , θ and σ^2 can be flexible, but it is advised to set a proper prior for either σ^2 or θ due to potential non-identifiability.

We employ a Gibbs sampling framework while handling each full conditional with different approaches. If the prior of β is normal $\beta \sim N(\beta_0, \Phi_0^{-1})$, then the posterior of β is also normal:

$$\beta|Y_{\mathcal{T}_1}, \hat{Z}_{\mathcal{T}_1}, \sigma^2 \sim N((\Phi_0 + X_{\mathcal{T}_1}^T X_{\mathcal{T}_1}/\sigma^2)^{-1}\{\Phi_0\beta_0 + X_{\mathcal{T}_1}^T(Y_{\mathcal{T}_1} - \hat{Z}_{\mathcal{T}_1})/\sigma^2\}, (\Phi_0 + X_{\mathcal{T}_1}^T X_{\mathcal{T}_1}/\sigma^2)^{-1}). \quad (12)$$

We then sample σ^2 from its full conditional. If the prior distribution for σ^2 is inverse gamma $\sigma^2 \sim \text{IG}(a_0, b_0)$, then the posterior of σ^2 is also inverse gamma:

$$\sigma^2|Y_{\mathcal{T}_1}, \hat{Z}_{\mathcal{T}_1}, \beta \sim \text{IG}\left(a_0 + n/2, b_0 + \|Y_{\mathcal{T}_1} - X_{\mathcal{T}_1}\beta - \hat{Z}_{\mathcal{T}_1}\|_2^2/2\right). \quad (13)$$

Denote the precision matrix of $\hat{Z}_{\mathcal{T}_1}|\theta$ from the RadGP prior as $\hat{\Phi}$. We sample the spatial random effects on \mathcal{T}_1 with conjugate gradients as illustrated in Nishimura & Suchard (2022), using the full conditional distribution:

$$\hat{Z}_{\mathcal{T}_1}|Y_{\mathcal{T}_1}, \beta, \sigma^2, \theta \sim N(\xi, (\hat{\Phi} + I_n/\sigma^2)^{-1}),$$

where $\xi = (\hat{\Phi} + I_n/\sigma^2)^{-1}(Y_{\mathcal{T}_1} - X_{\mathcal{T}_1}\beta)/\sigma^2$.

Finally, for the parameter θ in the covariance function K_θ , there is no available conjugate prior in general. We sample θ using the Metropolis-Hastings algorithm relying on the full conditional $p(\theta|\hat{Z}_{\mathcal{T}_1}) \propto p(\hat{Z}_{\mathcal{T}_1}|\theta)p(\theta)$. A detailed algorithm for posterior sampling can be found in Section S4.1 of the Supplementary Material.

If prediction on a test set is of interest, given MCMC samples of random effects on training set \mathcal{T}_1 and parameter θ , $Z_{\mathcal{T}_2}$ can be sampled from each unidimensional Gaussian distribution as in equation (11). Unlike most previous related work, this prediction accounts for dependence among test locations, which is important in many applied contexts.

In practical applications where the sample sizes of training set and test set are similar and much larger than the cardinality of parent sets, the computational complexity is $O(Mln_{\text{cg}}n)$, where l is the number of MCMC iterations, n_{cg} is the average number of conjugate gradient iterations, n is the sample size of training set, and M is the average number of nonzero elements per column in the RadGP precision matrix $\hat{\Phi}$. The derivation of computational complexity is in Section S4 of the Supplementary Material; here we discuss implications. The variable n_{cg} is determined by the distribution of eigenvalues of matrix $\hat{\Phi} + I_n/\sigma^2$ and numerical tolerance. The latter is fixed as 10^{-6} in our R package while the former is determined by the data set if the RadGP precision matrix $\hat{\Phi}$ approximates the original Gaussian process precision matrix Φ decently well. Therefore, the computational complexity is roughly proportional to M , the average number of nonzero elements per column in the precision matrix.

5. EXPERIMENTAL STUDIES

5.1. Approximation of a Gaussian Process Prior

Throughout Section 5, we consider the specific RadGP described in Section 2. We compare the RadGP prior with the nearest-neighbor Gaussian process (NNGP, Datta et al. 2016) implemented on a maximin ordering of the data (Guinness, 2018), in terms of their approximation accuracy. The true Gaussian process has mean zero and an isotropic Matérn covariance function

$$K_0(x) = \frac{\tau^2 2^{1-\nu}}{\Gamma(\nu)} (\phi x)^\nu \mathcal{K}_\nu(\phi x), \quad (14)$$

with the true parameters $(\phi, \tau^2, \nu) = (31.63, 1, 1.5)$. The value $\phi = 31.63$ is obtained by setting $K_0(0.15) = 0.05$, a choice suggested by Katzfuss et al. (2020). The experiment is carried out on a 40×40 grid in $[0, 1]^2$. According to the analysis of computational complexity in Section 4, we use the average number of nonzero elements per column in the precision matrix as a measure of complexity for both methods. The quality of approximation is measured by squared Wasserstein-2 distance between each approximate process and the true Gaussian process, which can be computed efficiently using the R package `transport` available from CRAN (Schuhmacher et al. 2024). As shown in Figure 2, the results are generally in favor of RadGP, as it achieves smaller approximation error under various complexity of the directed graphs.

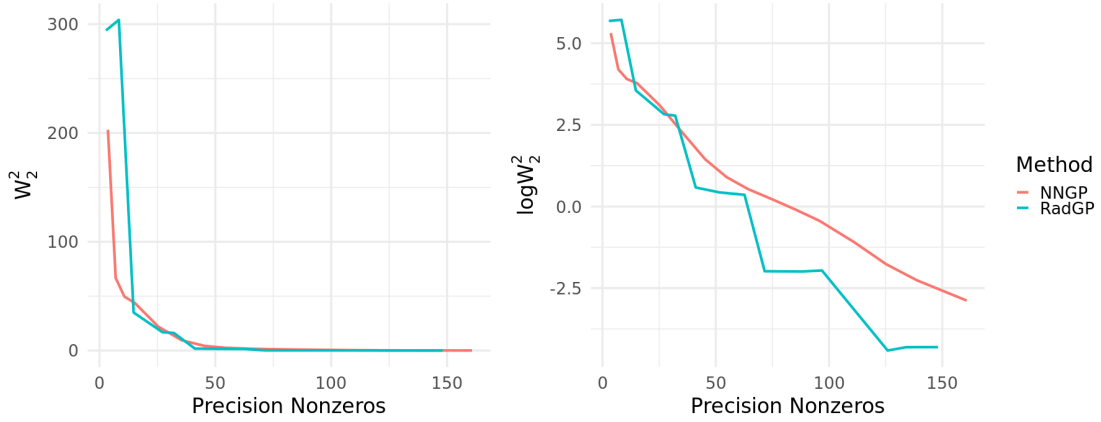


Fig. 2: Accuracy of approximating a Gaussian process prior. X-axis is the average number of nonzero elements per column in the precision matrix. Y-axis is the squared Wasserstein-2 distance and its logarithm.

5.2. Approximation of a Gaussian Process Regression Posterior

We study the performance of RadGP for the spatial regression model (10) with no covariates, where the true covariance function for spatial effects $Z(s)$ is the same as that in Section 5.1. The white noise $\epsilon(s)$ follows $N(0, \sigma^2)$ with $\sigma^2 = 0.01$. The parameters ϕ, τ^2, σ^2 are unknown and need to be estimated from training data, while the Matérn smoothness parameter $\nu = 3/2$ is assumed to be fixed and known. The domain is set as $\Omega = [0, 1]^2$, with training data consisting of 1600 grid locations in Ω . We replicate the analysis on 50 datasets. For each dataset, the test set is generated as 1000 random samples from the uniform distribution on Ω .

Three methods are compared: RadGP proposed in this paper, nearest-neighbor Gaussian process with maximin ordering, and Vecchia Gaussian process predictions (V-Pred) (Katzfuss et al., 2020) with maximin ordering. The last two methods share the same training procedure but differ in how they make predictions: NNGP assumes that testing locations are independent given the training locations whereas V-Pred allows dependencies among testing locations. All methods are fitted via the MCMC algorithm described in Section 4 and thus only differ in terms of their assumed graphs.

To measure the accuracy of approximations for prediction in the spatial regression model (10), we compute the Wasserstein-2 distance between the posterior predictive distributions from each of the three approximation methods and the true Gaussian process regression model. The Wasserstein-2 distance is computed using MCMC samples. The results are shown in Figure 3.

When the complexity of the directed graph is sufficiently large, NNGP and RadGP tend to have the same approximation error while V-Pred is slightly worse. However, RadGP is able to achieve the limiting approximation accuracy with a much smaller complexity compared to the other two methods, indicating a faster approximation by RadGP. Unlike prior approximation in Section 5.1, the posterior approximation error does not go to zero when the complexity of directed graphs increases. This nonzero error comes from two parts: first, the Gaussian process regression model (10) has unknown parameters that need to be estimated from a finite amount of data; second, the Wasserstein-2 distance computed based on a finite number of MCMC samples contains Monte Carlo error.

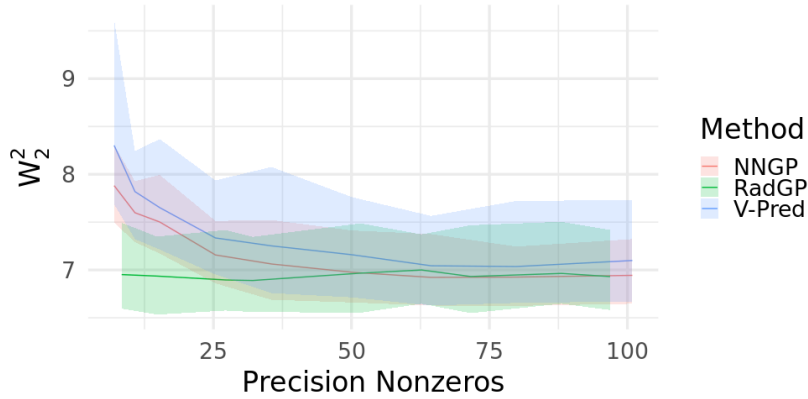


Fig. 3: Accuracy of approximating the posterior predictive distribution in Gaussian process regression. X-axis is the average number of nonzero elements per column in the precision matrix, and Y-axis is the squared Wasserstein-2 distance. Solid lines are mean values and shaded regions are 90% Bayesian credible intervals.

5.3. Surface Temperature Data

We consider the land surface temperature data on a $499\text{km} \times 581\text{km}$ region southeast of Addis Ababa in Ethiopia at April 1st, 2020. The data are a product of the MODIS (Moderate Resolution Imaging Spectroradiometer) instrument on the Aqua satellite. The original data set comes as a 499×581 image with each pixel corresponding to a $1\text{km} \times 1\text{km}$ spatial region, as shown in Fig. 5 left. However, atmosphere conditions like clouds can block earth surfaces, resulting in missing data for many pixels. There are 211,683 spatial locations with observed temperature values and 78,236 locations with missing values. We randomly split the training data into 3 folds, using two folds for training and one fold for out-of-sample validation. This results in a total of 141,122 training locations and 148,797 testing locations.

We consider the same Gaussian process regression model as Section 5.1 with no covariates, zero mean function and exponential covariance function $K_0(x) = \tau^2 \exp(-\phi x)$. The observed temperature values are centered to compensate for the lack of intercept term. We evaluate the performances of RadGP with radius 4.01km and nearest neighbor Gaussian process with neighbor size 15. The priors for both methods are set as $p(\phi) \propto 1$, $\tau^2 \sim \text{IG}(2, 1)$ and $\sigma^2 \sim \text{IG}(1, 0.1)$. Estimates for covariance parameters, out-of-sample mean squared errors and coverage for 95% credible intervals are shown in Table 1. The results are quite similar between the two methods.

The observed temperature and predicted temperature by RadGP are visualized in Fig. 5. In general, the land surface temperature changes smoothly with respect to geological locations. The

east and south part of the figure, which is covered by less vegetation, features slightly higher surface temperature. Small variations of temperature also occur in many local regions, indicating the geographical complexity of Ethiopia. There is a small blue plate in the west border of the figure that has significantly lower surface temperature than its surroundings, which corresponds to several lakes in the Great Rift Valley.

We further compare the performance of the two methods in terms of joint predictions at multiple held out locations. As we do not know the ground truth, we cannot calculate Wasserstein-2 error and instead focus on the joint likelihood ratio for held out data. Specifically, we select 567 pairs of locations in the set reserved for out-of-sample validation. Each pair consists of two locations with 1km distance from each other. Any two locations from different pairs are at least 10km apart. For each pair of locations, we compute the logarithm of the likelihood ratio between RadGP and NNGP. The distribution of the log likelihood ratio can provide important information about joint inference. Specifically, the mean of the log likelihood ratio is 2.152 and there are 68% pairs with positive log likelihood ratios. Since the distribution of the log likelihood ratio has heavy tails, we remove the bottom and top 5% of the values and visualize the rest in Fig. 4, where the red vertical line is ratio = 0. We can see in the majority of cases, RadGP performs better than NNGP in terms of characterizing dependencies between temperature at two close locations.

| | RadGP | NNGP |
|------------------------|----------------------|----------------------|
| $\phi \times 10^2$ | 5.761 (5.432, 6.133) | 5.689 (5.020, 6.321) |
| τ^2 | 1.706 (1.605, 1.807) | 1.744 (1.565, 1.972) |
| $\sigma^2 \times 10^3$ | 1.222 (1.104, 1.351) | 1.105 (0.994, 1.222) |
| MSE | 0.0761 | 0.0770 |
| coverage | 0.954 | 0.953 |
| time | 1929 sec | 1811 sec |

Table 1: Performance of RadGP and NNGP on land surface temperature data.

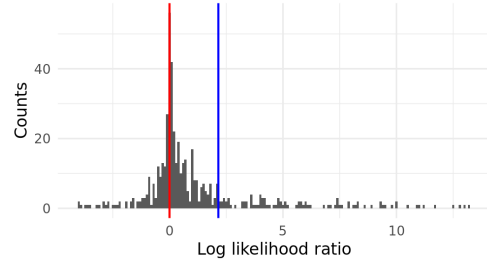


Fig. 4: Histogram of log likelihood ratio between RadGP and NNGP. The blue and red lines correspond to the mean log likelihood ratio value, and zero, respectively.

6. DISCUSSION

Vecchia approximations are arguably one of the most popular approaches for scaling up Gaussian process models to large datasets in spatial statistics. The major contribution of this article is to propose the first Vecchia-like approximation method that has strong theoretical guarantees in quantifying the accuracy of approximation to the original process. Our numerical experiments have shown competitive performance from the proposed RadGP compared to other Vecchia approximation methods. We have demonstrated that our method leads to improvements in characterizing joint predictive distributions while matching the performance of state-of-the-art methods in parameter estimation and marginal predictions.

Our current theory leads to several potential future research directions. First, we have established upper bounds for the approximation error to the original Gaussian process in Wasserstein-2 distance. We can further study lower bounds of this approximation error within specific families of approximations. It will be helpful to examine when the norm-controlled inversion bounds we

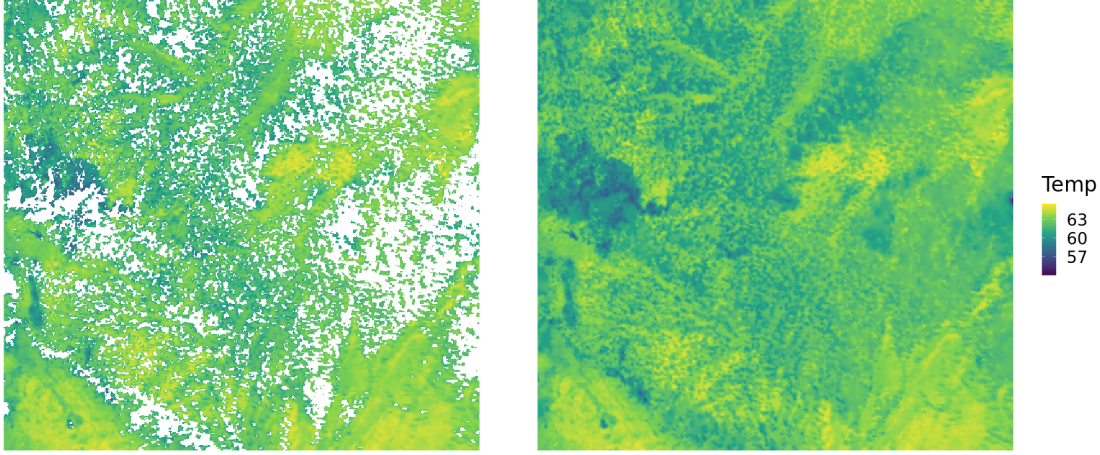


Fig. 5: Ethiopian land surface temperature on April 1st, 2020. Left: observed data; Right: predicted values from RadGP.

have used in the proofs are tight, and whether the derived conditions on the approximation radius ρ for various covariance functions in Corollary 1 can be made optimal for such families.

Second, existing Vecchia approximations that use maximin ordering (Katzfuss et al., 2020) systematically generate remote locations across the domain. While our theory shows close locations are effective in quantifying spatial dependence, it is still unclear whether and how remote locations help with the approximation of covariance function. We would like to expand our research into general Vecchia approximations. The objective is to study the approximation error for different approximation approaches and discover the optimal strategy that minimizes the approximation error under certain sparsity constraints.

Third, although our main focus has been on approximation of Gaussian processes, we can further consider how the approximate process will affect posterior estimation of model parameters, including spatial fixed effects and covariance parameters. Under our current theoretical framework, since the minimal separation distance q needs to be lower bounded, we can study Bayesian parameter estimation under increasing domain (Mardia & Marshall, 1984) or mixed domain (Lahiri & Zhu, 2006) asymptotic regimes. It remains an open problem whether our scalable approximation can maintain posterior consistency and optimal rates for all model parameters. We leave these directions for future exploration.

ACKNOWLEDGEMENTS

The authors thank Dr. Karlheinz Gröchenig for helpful discussion regarding the theory on norm-controlled inversion of Banach algebras, and two anonymous reviewers for detailed feedback and suggestion that greatly improved this article. Yichen Zhu has received funding from the European Research Council (ERC) under grant No. 101041064. Yichen Zhu, Michele Peruzzi and David Dunson have received funding from ERC under grant No. 856506 and United States National Institutes of Health under grant No. R01ES028804. Cheng Li has received funding from Singapore Ministry of Education Academic Research Funds Tier 1 Grant A-0004822-00-00. Part of this research was performed while Michele Peruzzi was visiting the Institute for Mathematical

and Statistical Innovation (IMSI), which is supported by the National Science Foundation (grant No. DMS-1929348).

SUPPLEMENTARY MATERIAL

Proofs of lemmas, theorems and corollaries, detailed algorithms, computational complexity analysis and additional experimental studies are available at *Supplementary Material for “Radial Neighbors for Provably Accurate Scalable Approximations of Gaussian Processes.”* An R package for regression models using radial neighbors Gaussian processes is available at <https://github.com/mkln/radgp>.

REFERENCES

- BAI, Y., SONG, P. X.-K. & RAGHUNATHAN, T. (2012). Joint composite estimating functions in spatiotemporal models. *Journal of the Royal Statistical Society: Series B (Statistical Methodology)* **74**, 799–824.
- BANERJEE, S., GELFAND, A. E., FINLEY, A. O. & SANG, H. (2008). Gaussian predictive process models for large spatial data sets. *Journal of the Royal Statistical Society: Series B (Statistical Methodology)* **70**, 825–848.
- BEVILACQUA, M., FAOUZI, T., FURRER, R. & PORCU, E. (2019). Estimation and prediction using generalized Wendland covariance functions under fixed domain asymptotics. *The Annals of Statistics* **47**, 828–856.
- BEVILACQUA, M. & GAETAN, C. (2015). Comparing composite likelihood methods based on pairs for spatial Gaussian random fields. *Statistics and Computing* **25**, 877–892.
- BURT, D., RASMUSSEN, C. E. & VAN DER WILK, M. (2020). Convergence of sparse variational inference in Gaussian processes regression. *Journal of Machine Learning Research* **21**, 1–63.
- CRESSIE, N. & JOHANNESSON, G. (2008). Fixed rank kriging for very large spatial data sets. *Journal of the Royal Statistical Society: Series B (Statistical Methodology)* **70**, 209–226.
- CRESSIE, N. A. C. (1993). *Statistics for Spatial Data*. Wiley-Interscience.
- DATTA, A., BANERJEE, S., FINLEY, A. O. & GELFAND, A. E. (2016). Hierarchical nearest-neighbor Gaussian process models for large geostatistical datasets. *Journal of the American Statistical Association* **111**, 800–812.
- EIDSVIK, J., SHABY, B. A., REICH, B. J., WHEELER, M. & NIEMI, J. (2014). Estimation and prediction in spatial models with block composite likelihoods. *Journal of Computational and Graphical Statistics* **23**, 295–315.
- FINLEY, A. O., DATTA, A., COOK, B. D., MORTON, D. C., ANDERSEN, H. E. & BANERJEE, S. (2019). Efficient algorithms for Bayesian nearest neighbor Gaussian processes. *Journal of Computational and Graphical Statistics* **28**, 401–414.
- FINLEY, A. O., SANG, H., BANERJEE, S. & GELFAND, A. E. (2009). Improving the performance of predictive process modeling for large datasets. *Computational Statistics & Data Analysis* **53**, 2873–2884.
- FURRER, R., GENTON, M. G. & NYCHYA, D. (2006). Covariance tapering for interpolation of large spatial datasets. *Journal of Computational and Graphical Statistics* **15**, 502–523.
- GELBRICH, M. (1990). On a formula for the L2 Wasserstein metric between measures on Euclidean and Hilbert spaces. *Mathematische Nachrichten* **147**, 185–203.
- GRAMACY, R. B. & APLEY, D. W. (2015). Local Gaussian process approximation for large computer experiments. *Journal of Computational and Graphical Statistics* **24**, 561–578.
- GUHANIYOGI, R., FINLEY, A. O., BANERJEE, S. & GELFAND, A. E. (2011). Adaptive Gaussian predictive process models for large spatial datasets. *Environmetrics* **22**, 997–1007.
- GUINNESS, J. (2018). Permutation and grouping methods for sharpening Gaussian process approximations. *Technometrics* **60**, 415–429.
- HEATON, M. J., DATTA, A., FINLEY, A., FURRER, R., GUHANIYOGI, R., GERBER, F., GRAMACY, R. B., HAMMERLING, D., KATZFUSS, M., LINDGREN, F., NYCHKA, D. W., SUN, F. & ZAMMIT-MANGION, A. (2019). A case study competition among methods for analyzing large spatial data. *Journal of Agricultural, Biological and Environmental Statistics* **24**, 398–425.
- JIN, B., PERUZZI, M. & DUNSON, D. B. (2021). Bag of DAGs: Flexible & scalable modeling of spatiotemporal dependence. *arXiv preprint arXiv: 2112.11870*.
- KATZFUSS, M. & GUINNESS, J. (2021). A general framework for Vecchia approximations of Gaussian processes. *Statistical Science* **36**, 124–141.
- KATZFUSS, M., GUINNESS, J., GONG, W. & ZILBER, D. (2020). Vecchia approximations of Gaussian-process predictions. *Journal of Agricultural, Biological and Environmental Statistics* **25**, 383–414.
- KAUFMAN, C. G., SCHERVISH, M. J. & NYCHKA, D. W. (2008). Covariance tapering for likelihood-based estimation in large spatial data sets. *Journal of the American Statistical Association* **103**, 1545–1555.
- KIDD, B. & KATZFUSS, M. (2022). Bayesian nonstationary and nonparametric covariance estimation for large spatial data (with discussion). *Bayesian Analysis* **17**, 291–351.

- LAHIRI, S. N. & ZHU, J. (2006). Resampling methods for spatial regression models under a class of stochastic designs. *The Annals of Statistics* **34**, 1774–1813.
- MARDIA, K. V. & MARSHALL, R. J. (1984). Maximum likelihood estimation of models for residual covariance in spatial statistics. *Biometrika* **71**, 135–146.
- NISHIMURA, A. & SUCHARD, M. A. (2022). Prior-preconditioned conjugate gradient method for accelerated Gibbs sampling in “large n, large p” Bayesian sparse regression. *Journal of the American Statistical Association* **118**, 2468–2481.
- PERUZZI, M., BANERJEE, S. & FINLEY, A. O. (2022). Highly scalable Bayesian geostatistical modeling via meshed Gaussian processes on partitioned domains. *Journal of the American Statistical Association* **117**, 969–982.
- PERUZZI, M. & DUNSON, D. B. (2022). Spatial multivariate trees for big data Bayesian regression. *Journal of Machine Learning Research* **23**, 1–40.
- PERUZZI, M. & DUNSON, D. B. (2024). Spatial meshing for general Bayesian multivariate models. *Journal of Machine Learning Research* **25**, 1–49.
- QUIÑONERO-CANDELA, J. & RASMUSSEN, C. E. (2005). A unifying view of sparse approximate Gaussian process regression. *Journal of Machine Learning Research* **6**, 1939–1959.
- RUE, H. (2001). Fast sampling of Gaussian markov random fields. *Journal of the Royal Statistical Society: Series B (Statistical Methodology)* **63**, 325–338.
- RUE, H. & HELD, L. (2005). *Gaussian Markov random fields: theory and applications*. Chapman and Hall/CRC.
- SANG, H., UN, M. & HUANG, J. Z. (2011). Covariance approximation for large multivariate spatial data sets with an application to multiple climate model errors. *Annals of Applied Statistics* **5**, 2519–2548.
- SCHÄFER, F., KATZFUSS, M. & OWHADI, H. (2021). Sparse Cholesky factorization by Kullback–Leibler minimization. *SIAM Journal on Scientific Computing* **43**, A2019–A2046.
- SCHUHMACHER, D., BÄHRE, B., BONNEEL, N., GOTTSCHLICH, C., HARTMANN, V., HEINEMANN, F., B., S. & SCHRIEBER, J. (2024). *transport: Computation of Optimal Transport Plans and Wasserstein Distances*. R package version 0.15-0.
- STEIN, M. L. (2014). Limitations on low rank approximations for covariance matrices of spatial data. *Spatial Statistics* **8**, 1–19.
- VECCHIA, A. V. (1988). Estimation and model identification for continuous spatial processes. *Journal of the Royal Statistical Society: Series B (Statistical Methodology)* **50**, 297–312.
- ZHANG, H. (2012). Asymptotics and computation for spatial statistics. In *Advances and Challenge in Space-time Modelling of Natural Events*. Springer.
- ZHANG, L., TANG, W. & SUDIPTO, B. (2023). Fixed-domain asymptotics under Vecchia’s approximation of spatial process likelihoods. *Statistica Sinica*, forthcoming.
- ZILBER, D. & KATZFUSS, M. (2021). Vecchia–Laplace approximations of generalized Gaussian processes for big non-Gaussian spatial data. *Computational Statistics & Data Analysis* **153**, 107081.

Supplementary material for “Radial Neighbors for Provably Accurate Scalable Approximations of Gaussian Processes”

BY YICHEN ZHU

Bocconi Institute for Data Science and Analytics, Bocconi University, Milan, MI, Italy.
 yichen.zhu@unibocconi.it

MICHELE PERUZZI

Department of Biostatistics, University of Michigan, Ann Arbor, Michigan, U.S.A.
 peruzzi@umich.edu

CHENG LI

Department of Statistics and Data Science, National University of Singapore, Singapore.
 stalic@nus.edu.sg

AND DAVID B. DUNSON

Department of Statistical Science & Mathematics, Duke University, North Carolina, U.S.A.
 dunson@duke.edu

This supplementary material is organized as follows. Section S1 includes the proof of lemma 1 in the main paper. Section S2 provides several auxiliary lemmas for our main theorems. The subsequent Section S3 states the proofs of Theorems 1 and 2 and Corollary 1 in the main paper. Section S4 provides the posterior sampling algorithms and computational complexity analysis for the RadGP regression model described in Section 4 of the main paper. Section S5 provides experimental studies that are not included in the main paper due to length limit. Section S6 provides further discussion on the relation between our RadGP theory and the existing tapering-based Gaussian process theory.

We define some notation that will be used throughout this supplementary material. The notation that is only used for specific lemmas will be defined before or in those lemmas. Let Ω be the spatial domain that is a connected subspace of \mathbb{R}^d . Let $Z = (Z_s : s \in \Omega)$ be a real valued Gaussian process on Ω with zero mean and covariance function $K : \Omega \times \Omega \rightarrow \mathbb{R}$, and let \hat{Z} be the radial neighborhood Gaussian process (RadGP) on Ω . Let $\mathcal{D} \subset \Omega$ be an arbitrary finite subset of Ω . Without loss of generality, we index the elements of \mathcal{D} as $\mathcal{D} = \{w_1, w_2, \dots, w_n\}$, such that for any $w_i \in \mathcal{D}$, all locations in $\text{pa}(w_i)$ precede w_i in the order prescribed by the radial neighbors graph in Section 2.2 of the main text. For any index $i = 1, \dots, n$, let $\nu(i) = \{j \in \mathbb{N} : j < i\}$ be the collection of indices that are smaller than i . Since Ω can be an uncountable set, we use s to denote a generic spatial location of Ω . In the context where a directed graph exists, we use $\text{pa}(s)$ to denote the parent set of s .

For a finite set $A \subset \Omega$, let Z_A be the finite-dimensional random variable of the process Z on A . For two finite sets $A, B \subset \Omega$, we denote the covariance matrix between Z_A and Z_B as Σ_{AB} . For a generic square matrix C , let $\lambda_{\min}(C)$ and $\lambda_{\max}(C)$ be its smallest and largest eigenvalues. The matrix l_1 , l_2 and trace norms are denoted by $\|\cdot\|_1$, $\|\cdot\|_2$ and $\|\cdot\|_{\text{tr}}$. The vector l_1 and l_2

norms are denoted using the same notation as the matrix norms. Finally, for simplicity, we denote $(\hat{\Sigma}_{\mathcal{D}\mathcal{D}})^{-1}$ as $\hat{\Phi}$.

S1. PROOF OF LEMMA 1

Proof. By the Kolmogorov extension theorem, $\hat{Z}(\cdot)$ defines a stochastic process if its finite density $p(\hat{Z}_A)$ on any finite set $A \subset \Omega$ defined in Equation (3) of the main paper satisfies the following two conditions:

- (C1) For all finite set $A \subset \Omega$, let \tilde{A} be a permutation of elements in A , then $p(\hat{Z}_{\tilde{A}}) = p(\hat{Z}_A)$;
 (C2) For all finite sets $A, A' \subset \Omega$ with $A \cap A' = \emptyset$, $\int p(\hat{Z}_{A \cup A'}) \prod_{s \in A'} ds = p(\hat{Z}_A)$.

We verify these two conditions for the radial neighbors Gaussian process, defined in Equations (1), (2) and (3) of the main text.

CONDITION C1 This essentially requires that for all $A \subset \Omega$, Equation (3) in the main paper defines a valid finite dimensional distribution. In the following, we prove a stronger condition that for any finite set $A \subseteq \Omega$, the distribution on A defined by Equation (3) in the main paper is a Gaussian distribution.

Let $u_1 \in \mathbb{R}^{d_1}$, $u_2 \in \mathbb{R}^{d_2}$ be two random vectors. If $u_1 \in N(\mu_1, \Sigma_1)$, $u_2|u_1 \sim N(\mu_2 + B(u_2 - \mu_1), \Sigma_2)$, then (u_2, u_1) follows a joint Gaussian distribution.

This claim can be verified by direct calculation and its proof is omitted. We now show \hat{Z}_A follows a Gaussian distribution. Recall the notations in the main paper that $A = U \cup V$ with $U \subset \Omega \setminus \mathcal{D}$ and $V \subset \mathcal{D}$. By the claim, $p(\hat{Z}_{\mathcal{D}}) = \prod_{i=1}^n p(\hat{Z}_{w_i} | \hat{Z}_{\text{pa}(w_i)})$ follows a joint Gaussian distribution. Similarly, since for all $s \in U$, $\text{pa}(s) \subset \mathcal{D}$ and $\hat{Z}_{\mathcal{D} \cup U} = p(\hat{Z}_{\mathcal{D}}) \prod_{s \in U} p(\hat{Z}_s | \text{pa}(s))$, we have $\hat{Z}_{\mathcal{D} \cup U}$ also follows a Gaussian distribution. Noticing that \hat{Z}_A can be obtained from $\hat{Z}_{\mathcal{D} \cup U}$ by integrating out $Z_{w_i}, \forall i \in \mathcal{D} \setminus A$, we conclude \hat{Z}_A also follows a Gaussian distribution.

CONDITION C2 Since A' is a finite set, it suffices to prove condition C2 when $A' = \{x\}$ for arbitrary finite set $A \subset \Omega$ and $x \in \Omega \setminus A$. We split the proof into two cases: $x \in \mathcal{D}$ and $x \in \Omega \setminus \mathcal{D}$.

For $x \in \mathcal{D}$, by definition,

$$\begin{aligned} p(\hat{Z}_A) &= \int p(\hat{Z}_U | \hat{Z}_{\mathcal{D}}) \prod_{i=1}^n p(\hat{Z}_{w_i} | \hat{Z}_{\text{pa}(w_i)}) \prod_{w_i \in \mathcal{D} \setminus V} dw_i \\ &= \int \left\{ \int p(\hat{Z}_U | \hat{Z}_{\mathcal{D}}) \prod_{i=1}^n p(\hat{Z}_{w_i} | \hat{Z}_{\text{pa}(w_i)}) \prod_{w_i \in \mathcal{D} \setminus (V \cup \{x\})} dw_i \right\} dx \\ &= \int p(\hat{Z}_{A \cup \{x\}}) dx. \end{aligned}$$

For $x \in \Omega \setminus \mathcal{D}$, since x is independent of all other locations when conditional on \mathcal{D} , we have

$$\begin{aligned} p(\hat{Z}_A) &= \int p(\hat{Z}_U | \hat{Z}_{\mathcal{D}}) \prod_{i=1}^n p(\hat{Z}_{w_i} | \hat{Z}_{\text{pa}(w_i)}) \prod_{w_i \in \mathcal{D} \setminus V} dw_i \\ &= \int \left\{ \int p(\hat{Z}_U | \hat{Z}_{\mathcal{D}}) \prod_{i=1}^n p(\hat{Z}_{w_i} | \hat{Z}_{\text{pa}(w_i)}) \prod_{w_i \in \mathcal{D} \setminus V} dw_i \right\} p(\hat{Z}_x | \hat{Z}_{\mathcal{D}}) dx \end{aligned}$$

$$= \int p(\hat{Z}_{A \cup \{x\}}) dx.$$

CONCLUSION Using the Kolmogorov extension theorem, we conclude that \hat{Z} is a well-defined stochastic process. Since we have also verified each finite-dimensional distribution of \hat{Z} is Gaussian, we further conclude that \hat{Z} is a valid Gaussian process. \square

S2. AUXILIARY LEMMAS FOR MAIN THEOREMS

S2.1. Upper Bound for W_2 Distance

We begin our theoretical analysis by studying the upper bound for the quantity of interest, the Wasserstein-2 distance. Let a decomposition of $\Sigma_{\mathcal{D}\mathcal{D}}^{-1}$ be $\Sigma_{\mathcal{D}\mathcal{D}}^{-1} = LL^T$ with $L = (l_1, \dots, l_n)$; similarly let $\hat{\Phi} = \hat{L}\hat{L}^T$ with $\hat{L} = (\hat{l}_1, \dots, \hat{l}_n)$. For a generic $m \times m$ symmetric matrix A , let $\lambda_{\max}(A)$ be its largest eigenvalue. For a generic $k \times m$ matrix B , let $\|B\|_2 = \{\lambda_{\max}(B^T B)\}^{1/2}$ and $\|B\|_{\text{tr}} = \text{tr}\{(B^T B)^{1/2}\}$.

LEMMA S1. *For any decomposition $\Sigma_{\mathcal{D}\mathcal{D}}^{-1} = LL^T$ and $\hat{\Phi} = \hat{L}\hat{L}^T$, if $\|\hat{L} - L\|_2 \leq \|\Sigma_{\mathcal{D}\mathcal{D}}\|_2^{-1/2}/2$, then we have*

$$\begin{aligned} W_2^2(Z_{\mathcal{D}}, \hat{Z}_{\mathcal{D}}) &\leq \|\Sigma_{\mathcal{D}\mathcal{D}} - \hat{\Sigma}_{\mathcal{D}\mathcal{D}}\|_{\text{tr}} \\ &\leq 8n\|\Sigma_{\mathcal{D}\mathcal{D}}\|_2^2 \left(2 \max_i \|l_i\|_2 \max_i \|\hat{l}_i - l_i\|_2 + \max_i \|\hat{l}_i - l_i\|_2^2\right). \end{aligned}$$

Proof. By Proposition 1 of Quang (2023), we have

$$W_2^2(Z_{\mathcal{D}}, \hat{Z}_{\mathcal{D}}) \leq \|\Sigma_{\mathcal{D}\mathcal{D}} - \hat{\Sigma}_{\mathcal{D}\mathcal{D}}\|_{\text{tr}}. \quad (\text{S1})$$

Thus, it suffices to derive the upper bound for $\|\Sigma_{\mathcal{D}\mathcal{D}} - \hat{\Sigma}_{\mathcal{D}\mathcal{D}}\|_{\text{tr}}$. Plugging in the decomposition of $\Sigma_{\mathcal{D}\mathcal{D}}^{-1}$ and $\hat{\Phi}$, we have that

$$\begin{aligned} \Sigma_{\mathcal{D}\mathcal{D}} - \hat{\Sigma}_{\mathcal{D}\mathcal{D}} &= \Sigma_{\mathcal{D}\mathcal{D}}(\hat{\Phi} - \Sigma_{\mathcal{D}\mathcal{D}}^{-1})\hat{\Phi}^{-1} \\ &= \Sigma_{\mathcal{D}\mathcal{D}}(\hat{L}\hat{L}^T - LL^T)\hat{\Phi}^{-1} \\ &= \sum_{i=1}^n \left\{ \Sigma_{\mathcal{D}\mathcal{D}} \hat{l}_i (\hat{\Phi}^{-1} \hat{l}_i)^T - \Sigma_{\mathcal{D}\mathcal{D}} l_i (\hat{\Phi}^{-1} l_i)^T \right\}. \end{aligned} \quad (\text{S2})$$

We need an auxiliary result regarding the trace norm of matrix operations.

Technical Lemma S1. For any $u_1, u_2, v_1, v_2 \in \mathbb{R}^n$, we have

$$\|u_2 v_2^T - u_1 v_1^T\|_{\text{tr}} \leq 2(\|u_2 - u_1\|_2 \|v_1\|_2 + \|v_2 - v_1\|_2 \|u_1\|_2 + \|u_2 - u_1\|_2 \|v_2 - v_1\|_2).$$

Proof. We first decompose the l_2 norm of $u_2 v_2^T - u_1 v_1^T$ as

$$\|u_2 v_2^T - u_1 v_1^T\| \leq \|u_2 - u_1\|_2 \|v_1\|_2 + \|v_2 - v_1\|_2 \|u_1\|_2 + \|u_2 - u_1\|_2 \|v_2 - v_1\|_2.$$

Since the right eigenvectors corresponding to nonzero singular values of matrix $u_2 v_2^T - u_1 v_1^T$ must lie in a rank two space $\text{span}\{v_1, v_2\}$, there are at most two nonzero singular values for this matrix. Therefore

$$\|u_2 v_2^T - u_1 v_1^T\|_{\text{tr}} \leq 2\|u_2 v_2^T - u_1 v_1^T\|_2$$

Combining the above two equations completes the proof. \square

We now use the result of Technical Lemma S1 and plug Equation (S2) into Equation (S1) to derive that

$$\begin{aligned}
\|\Sigma_{\mathcal{D}\mathcal{D}} - \hat{\Sigma}_{\mathcal{D}\mathcal{D}}\|_{\text{tr}} &\leq \sum_{i=1}^n \|\Sigma_{\mathcal{D}\mathcal{D}} \hat{l}_i (\hat{\Phi}^{-1} \hat{l}_i)^T - \Sigma_{\mathcal{D}\mathcal{D}} l_i (\hat{\Phi}^{-1} l_i)^T\|_{\text{tr}} \\
&\leq \sum_{i=1}^n 2 \left\{ \|\Sigma_{\mathcal{D}\mathcal{D}} (\hat{l}_i - l_i)\|_2 \|\hat{\Phi}^{-1} l_i\|_2 + \|\Sigma_{\mathcal{D}\mathcal{D}} l_i\|_2 \|\hat{\Phi}^{-1} (\hat{l}_i - l_i)\|_2 \right. \\
&\quad \left. + \|\Sigma_{\mathcal{D}\mathcal{D}} (\hat{l}_i - l_i)\|_2 \|\hat{\Phi}^{-1} (\hat{l}_i - l_i)\|_2 \right\} \\
&\leq \sum_{i=1}^n 2 \|\Sigma_{\mathcal{D}\mathcal{D}}\|_2 \|\hat{\Phi}^{-1}\|_2 (2 \|\hat{l}_i - l_i\|_2 \|l_i\|_2 + \|\hat{l}_i - l_i\|_2^2) \\
&\leq 2n \|\Sigma_{\mathcal{D}\mathcal{D}}\|_2 \|\hat{\Phi}^{-1}\|_2 (2 \max_i \|\hat{l}_i - l_i\|_2 \max_i \|l_i\|_2 + \max_i \|\hat{l}_i - l_i\|_2^2).
\end{aligned}$$

If $\|\hat{L} - L\|_2 \leq \|\Sigma_{\mathcal{D}\mathcal{D}}\|_2^{-1/2}/2$, then we have that $\lambda_{\min}(\hat{L}) \geq \lambda_{\min}(L)/2$ and hence $\lambda_{\min}(\hat{\Phi}) \geq \lambda_{\min}\{(\Sigma_{\mathcal{D}\mathcal{D}})^{-1}\}/4$. This gives the upper bound $4\|\hat{\Phi}^{-1}\|_2 \leq \|\Sigma_{\mathcal{D}\mathcal{D}}\|_2$. Thus

$$\|\Sigma_{\mathcal{D}\mathcal{D}} - \hat{\Sigma}_{\mathcal{D}\mathcal{D}}\|_{\text{tr}} \leq 8n \|\Sigma_{\mathcal{D}\mathcal{D}}\|_2^2 (2 \max_i \|\hat{l}_i - l_i\|_2 \max_i \|l_i\|_2 + \max_i \|\hat{l}_i - l_i\|_2^2).$$

□

S2.2. Matrix Norms

Following the upper bound of Wasserstein distance in Lemma S1, we provide estimates for various matrix norms that are related to this upper bound.

LEMMA S2. *The following bounds regarding the set \mathcal{D} hold:*

(1) *If $Z \in \mathcal{Z}_{v_r}$ for some $r > 0$, then*

$$\|\Sigma_{\mathcal{D}\mathcal{D}}\|_2 \leq \|\Sigma_{\mathcal{D}\mathcal{D}}\|_1 \leq 1 + d2^d q^{-d} \int_{q/2}^1 x^{d-1} \frac{1}{v_r(x - q/2)\{1 + (x - q/2)^2\}} dx.$$

(2) *If $Z \in \mathcal{Z}_{c_r}$ for some $r \geq d + 1$, then*

$$\|\Sigma_{\mathcal{D}\mathcal{D}}\|_2 \leq \|\Sigma_{\mathcal{D}\mathcal{D}}\|_1 \leq 1 + d2^d q^{-d} \max\{1, (q/2)^{d-1}\}.$$

(3) *Let $c_2 = 12 \{\pi \Gamma^2(d/2 + 1)/9\}^{1/(d+1)}$, $c_1 = 2\Gamma(d/2 + 1)(2^{3/2}/c_2)^d$ and $\phi_0(c_2/q) = \inf_{\|\omega\|_2 \leq 2c_2/q} \hat{K}_0(\omega)$ with \hat{K}_0 being the Fourier transform of d -dimensional function K_0 , then*

$$\|\Sigma_{\mathcal{D}\mathcal{D}}^{-1}\|_2 \leq c_1 \{\phi_0(c_2/q')\}^{-1} q'^d, \quad \text{for all } q' \leq q.$$

(4) *If $Z \in \mathcal{Z}_{v_r}$ for some $r > 0$, then $\|\Sigma_{\mathcal{D}\mathcal{D}}\|_{v_r, l} \leq 2^d q^{-d} (1 + q/2)^{d-1} (1 + q/2 + d)$ for all $l \in \mathbb{N}$.*

(5) *If $Z \in \mathcal{Z}_{c_r}$ for some $r \geq d + 1$, then $\|\Sigma_{\mathcal{D}\mathcal{D}}\|_{c_r - (d+1)/2} \leq d2^{d-1} \pi / \sqrt{6}$.*

Proof. (1) Since the matrix l_2 norm is bounded by the matrix l_1 norm, we have

$$\|\Sigma_{\mathcal{D}\mathcal{D}}\|_2 \leq \|\Sigma_{\mathcal{D}\mathcal{D}}\|_1 = \sup_i \sum_{j=1}^n K(w_i, w_j). \quad (\text{S3})$$

Now consider the term $\sum_{j=1}^n K(w_i, w_j)$. Recall that $q = \min_{1 \leq i < j \leq |\mathcal{D}|} \|w_i - w_j\|$ is the minimal separation distance among all locations in \mathcal{D} . Define an auxiliary function $\varphi : \Omega \rightarrow \Omega$ such

that (1) $\|\varphi(s) - s\|_2 < q/2$; (2) If there exists some $w_i \in \mathcal{D}$ such that $\|w_i - s\| < q/2$, then $\varphi(s) = w_i$.

The function φ maps the unit ball $U(w_i, q/2)$, $1 \leq i \leq n$ into a singleton $\{w_i\}$. We extend the definition of $v_r(\cdot)$ to $(-\infty, 0)$ by letting $v_r(x) = 1$ for all $x < 0$. Then we have that

$$\begin{aligned}
\sum_{j=1}^n K(w_i, w_j) &= \frac{1}{\pi^{d/2}(q/2)^d/\Gamma(d/2+1)} \int_{s \in \bigcup_{j=1}^n U(w_j, q/2)} K(w_i, w_j) ds \\
&= \frac{1}{\pi^{d/2}(q/2)^d/\Gamma(d/2+1)} \int_{s \in \bigcup_{j=1}^n U(w_j, q/2)} K(w_i, \varphi(s)) ds \\
&\leq \frac{\Gamma(d/2+1)2^d}{\pi^{d/2}q^d} \int_{s \in \Omega} K(w_i, \varphi(s)) ds \\
&\leq \frac{\Gamma(d/2+1)2^d}{\pi^{d/2}q^d} \int_{s \in \Omega} \frac{1}{v_r(\max\{0, \|s\|_2 - q/2\})[1 + \{\max(0, \|s\|_2 - q/2)\}^{d+1}]} ds \\
&\stackrel{\Omega \subset \mathbb{R}^d}{\leq} \frac{\Gamma(d/2+1)2^d}{\pi^{d/2}q^d} \int_0^{+\infty} \frac{2\pi^{d/2}x^{d-1}}{\Gamma(d/2)} \\
&\quad \times \frac{1}{v_r(\max\{0, x - q/2\})[1 + \{\max(0, x - q/2)\}^{d+1}]} dx \\
&= 1 + d2^d q^{-d} \int_{q/2}^{+\infty} \frac{x^{d-1}}{v_r(x - q/2)\{1 + (x - q/2)^{d+1}\}} dx, \tag{S4}
\end{aligned}$$

Combining equations (S3) and (S4), we finish the proof.

(2) Using the same notation as the proof of (1) above, we have

$$\begin{aligned}
\sum_{j=1}^n K(w_i, w_j) &\leq \frac{\Gamma(d/2+1)2^d}{\pi^{d/2}q^d} \int_{s \in \Omega} K(w_i, \varphi(s)) ds \\
&\leq \frac{\Gamma(d/2+1)2^d}{\pi^{d/2}q^d} \int_{s \in \Omega} \frac{1}{(1 + \max\{0, \|s\|_2 - q/2\})^r} ds \\
&\stackrel{\Omega \subset \mathbb{R}^d}{\leq} \frac{\Gamma(d/2+1)2^d}{\pi^{d/2}q^d} \int_0^{+\infty} \frac{2\pi^{d/2}x^{d-1}}{\Gamma(d/2)} \frac{1}{(1 + \max\{0, \|x\|_2 - q/2\})^r} dx \\
&= 1 + d2^d q^{-d} \int_{q/2}^{+\infty} \frac{x^{d-1}}{(1 + x - q/2)^r} dx \\
&\stackrel{r \geq d+1}{\leq} 1 + d2^d q^{-d} \max\{1, (q/2)^{d-1}\}.
\end{aligned}$$

(3) The conclusion follows directly from Theorem 12.3 of Wendland (2004).

(4) For a vector $w \in \mathbb{R}^d$, we use $w[j]$ to denote its j th component. We have that for any $l \in \mathbb{N}$,

$$\begin{aligned}
\|\Sigma_{\mathcal{D}\mathcal{D}}\|_{v_r, l} &= \sum_{k=0}^{+\infty} \frac{1}{(k!)^r} \|\nabla_l^k(\Sigma)\|_2 \\
&\leq \sum_{k=0}^{+\infty} \frac{1}{(k!)^r} \|\nabla_l^k(\Sigma)\|_1
\end{aligned}$$

$$\begin{aligned}
&= \sum_{k=0}^{+\infty} \frac{1}{(k!)^r} \sup_i \sum_{j=1}^n |w_i[l] - w_j[l]|^k K(w_i, w_j) \\
&\leq \sum_{k=0}^{+\infty} \frac{1}{(k!)^r} \sup_i \sum_{j=1}^n |w_i[l] - w_j[l]|^k \frac{1}{v_r(\|w_i - w_j\|_2)(\|w_i - w_j\|_2^2 + 1)} \\
&= \sup_i \sum_{j=1}^n \frac{v_r(|w_i[l] - w_j[l]|)}{v_r(\|w_i - w_j\|_2)(\|w_i - w_j\|_2^2 + 1)} \\
&\leq \sup_i \sum_{j=1}^n \frac{1}{\|w_i - w_j\|^{d+1} + 1}.
\end{aligned}$$

Using the same trick as in the proof of (1) to turn the summation into an integration, we have that

$$\begin{aligned}
&\sup_i \sum_{j=1}^n \frac{1}{\|w_i - w_j\|^{d+1} + 1} \\
&= \frac{1}{\pi^{d/2}(q/2)^d/\Gamma(d/2 + 1)} \int_{s \in \bigcup_{j=1}^n U(w_j, q/2)} \frac{1}{\|w_i - \varphi(s)\|^{d+1} + 1} ds \\
&\leq \frac{\Gamma(d/2 + 1)2^d}{\pi^{d/2}q^d} \int_{s \in \Omega} \frac{1}{\|w_i - \varphi(s)\|^{d+1} + 1} ds \\
&\leq d2^d q^{-d} \int_0^{+\infty} \frac{x^{d-1}}{(\max\{0, x - q/2\})^2 + 1} dx \\
&\leq d2^d q^{-d} \left\{ \int_0^{1+q/2} x^{d-1} dx + \int_{1+q/2}^{+\infty} \frac{x^{d-1}}{(x - q/2)^{d+1}} dx \right\} \\
&\leq 2^d q^{-d} (1 + q/2)^d + d2^d q^{-d} (1 + q/2)^{d-1} \int_{1+q/2}^{+\infty} \frac{1}{(x - q/2)^2} dx \\
&= 2^d q^{-d} (1 + q/2)^d + d2^d q^{-d} (1 + q/2)^{d-1} \\
&= 2^d q^{-d} (1 + q/2)^{d-1} (1 + q/2 + d).
\end{aligned}$$

(5)

$$\begin{aligned}
\|\Sigma_{\mathcal{DD}}\|_{c_{r-(d+1)/2}} &\leq \left\{ \sum_{k \in \mathbb{Z}^d} \sup_{w_i, w_j \in \mathcal{D}} (1 + \|w_i - w_j\|_\infty)^{-2r} \right. \\
&\quad \left. \times (1 + \|w_i - w_j\|_\infty)^{2(r-(d+1)/2)} \mathbb{1}_{\{w_i - w_j \in [0,1)^{d+k}\}} \right\}^{\frac{1}{2}} \\
&\leq \left\{ \sum_{k \in \mathbb{Z}^d} \sup_{s \in [0,1)^{d+k}} (1 + \|s\|_\infty)^{-(d+1)} \right\}^{\frac{1}{2}} \\
&\leq \left\{ \sum_{k=1}^{\infty} [(2k)^d - \{2(k-1)\}^d] k^{-(d+1)} \right\}^{\frac{1}{2}}
\end{aligned}$$

$$\begin{aligned}
&\leq \left\{ \sum_{k=1}^{\infty} d(2k)^{d-1} k^{-(d+1)} \right\}^{\frac{1}{2}} \\
&= d2^{d-1} \left(\sum_{k=1}^{\infty} k^{-2} \right)^{\frac{1}{2}} = d2^{d-1} \frac{\pi}{\sqrt{6}}.
\end{aligned}$$

□

S2.3. Bounds regarding Matrix Inversion

To utilize the upper bound proved in Lemma S1, it is necessary to bound the quantity $\max_i \|l_i - \hat{l}_i\|_2$, which involves the Cholesky decomposition of an inverse matrix. In this section, we present some general tools that describe the properties of matrix inversion in some norms.

We first discuss the Cholesky decomposition that yields matrix L and \hat{L} . We introduce the notation of quoting a submatrix by its indices that will only be used in this subsection. For a generic matrix B , let $B[i, j]$ be its entry at the i th row and j th column. Recall $\nu(i) = \{j \in \mathbb{N} : j < i\}$, further define $N(i) = \{j \in \nu(i) : \|w_i - w_j\|_2 < \rho\}$. Our directed acyclic graphs constructed in Section 2.3 of the main text induce the following decomposition of the precision matrices $\Sigma_{\mathcal{D}\mathcal{D}}^{-1}$ from the original Gaussian processes and $\hat{\Phi}$ from the radial neighbors Gaussian processes.

LEMMA S3. *The precision matrices $\Sigma_{\mathcal{D}\mathcal{D}}^{-1}$ and $\hat{\Phi}$ satisfy*

$$\Sigma_{\mathcal{D}\mathcal{D}}^{-1} = (I_n - B^T)D^{-1}(I_n - B), \quad \hat{\Phi} = (I_n - \hat{B}^T)\hat{D}^{-1}(I_n - \hat{B}),$$

where B and \hat{B} are lower triangular matrices such that

$$B[\nu(i), i] = (\Sigma[\nu(i), \nu(i)])^{-1} \Sigma[\nu(i), i] \quad \text{and} \quad B[j, i] = 0, \quad \forall j \notin \nu(i),$$

$$\hat{B}[N(i), i] = (\Sigma[N(i), N(i)])^{-1} \Sigma[N(i), i] \quad \text{and} \quad \hat{B}[j, i] = 0, \quad \forall j \notin N(i).$$

D and \hat{D} are diagonal matrices, such that

$$D[i, i] = K(w_i, w_i) - \Sigma[\nu(i), i]^T (\Sigma[\nu(i), \nu(i)])^{-1} \Sigma[\nu(i), i],$$

$$\hat{D}[i, i] = K(w_i, w_i) - \Sigma[N(i), i]^T (\Sigma[N(i), N(i)])^{-1} \Sigma[N(i), i].$$

Proof. Radial neighbors Gaussian process implies an algorithm to find a sparse approximation for the Cholesky of the inverse of a matrix. We begin by constructing the exact decomposition $\Sigma_{\mathcal{D}\mathcal{D}}^{-1} = LL^T$ with $L = (l_1, \dots, l_n)$. By Bayes' rule, the joint density of $Z_{\mathcal{D}}$ can be decomposed as

$$p(Z_{\mathcal{D}}) = p(Z_{w_1}) \prod_{i=2}^N p(Z_{w_i} | Z_{w_1}, \dots, Z_{w_{i-1}}). \quad (\text{S5})$$

The decomposition of density induces a decomposition on the precision matrix of Gaussian distribution $p(Z_{\mathcal{D}})$. Specifically, writing (S5) in the form of conditional regression, we have

$$Z_{w_1} = \eta_1, \quad Z_{w_i} = \sum_{j=1}^{i-1} b_{i,j} Z_{w_j} + \eta_i, \quad \text{for all } 2 \leq i \leq n,$$

where $b_{i,j}, 1 \leq j \leq i-1$ are conditional regression coefficients satisfying

$$[b_{i,1} \ b_{i,2} \ \cdots \ b_{i,i-1}]^T = (\Sigma[\nu(i), \nu(i)])^{-1} \Sigma[\nu(i), i]$$

and $\eta_i, 1 \leq i \leq n$ are independent mean zero Gaussian random variables with variance

$$\text{Var}(\eta_i) = \text{Var}(Z_{w_i} | Z_{w_1}, \dots, Z_{w_{i-1}}) = K(w_i, w_i) - (\Sigma[\nu(i), i])^T (\Sigma[\nu(i), \nu(i)])^{-1} \Sigma[\nu(i), i].$$

Define the coefficient matrix B such that $B[i, j] = b_{i,j}$ if and only if $i > j$ and $B[i, j] = 0$ otherwise. That is, $B[i, \nu(i)]^T = (\Sigma[\nu(i), \nu(i)])^{-1} \Sigma[\nu(i), i]$. Also define a diagonal matrix D such that $D[i, i] = \text{Var}(\eta_i)$. Then by the equality $w = Bw + \eta$, we have that

$$\Sigma_{\mathcal{D}\mathcal{D}}^{-1} = (I_n - B^T)D^{-1}(I_n - B).$$

To obtain the decomposition $\Sigma_{\mathcal{D}\mathcal{D}}^{-1} = LL^T$, we let L be

$$L = (I_n - B^T)D^{-1/2}.$$

This has proved the first decomposition in Lemma S3.

For the decomposition of the precision matrix $\hat{\Phi}$ of \hat{Z} , we now use a similar way to derive the decomposition of $\hat{\Phi}$. Noticing the definition of ordering $(w_i)_{1 \leq i \leq n}$ implies $\text{pa}(w_i) \subset \nu(i)$, we have

$$p(\hat{Z}_{\mathcal{D}}) = p(\hat{Z}_{w_1}) \prod_{i=2}^n p(\hat{Z}_{w_i} | \hat{Z}_{\text{pa}(w_i)}).$$

Denote $N(i) = \{j \in \nu(i) : \|w_i - w_j\|_2 < \rho\}$. The above equation similarly induces a decomposition of $\hat{\Phi}_{\mathcal{D}\mathcal{D}}$ as

$$\hat{\Phi}_{\mathcal{D}\mathcal{D}} = (I_n - \hat{B}^T)\hat{D}^{-1}(I_n - \hat{B}),$$

where \hat{B} is an $n \times n$ matrix such that $\hat{B}[i, j] = 0$ for all $j \notin N(i)$. For the nonzero elements of \hat{B} , we have for all $1 \leq i \leq n$

$$\hat{B}[i, N(i)]^T = \Sigma_{N(i), N(i)}^{-1} \Sigma_{N(i), i}.$$

The matrix \hat{D} is a diagonal matrix with entries

$$\hat{D}[i, i] = K(w_i, w_i) - \Sigma_{N(i), i}^T \Sigma_{N(i), i}^{-1} \Sigma_{N(i), i}.$$

The matrix decomposition $\hat{\Phi} = \hat{L}\hat{L}^T$ is defined by

$$\hat{L} = (I_n - \hat{B}^T)\hat{D}^{-1/2}.$$

□

We next introduce a result from literature of norm-controlled inversion of Banach Algebra that helps us transfer the spatial decay properties from covariance matrices to precision matrices and the Cholesky of precision matrices.

Specifically, let the matrix $A \in \mathbb{R}^{n \times n}$ be associated with n spatial locations w_1, \dots, w_n such that the (i, j) -entry of A , denoted by $A[i, j]$, is a function of the difference $w_i - w_j$. Let $w_i[l]$ be the l th coordinate of w_i . For all $1 \leq l \leq d$, define a linear matrix operator ∇_l such that

$$\nabla_l(A)[i, j] = (w_i[l] - w_j[l])A[i, j].$$

For such a square matrix A , we define its l th order v_r norm and c_r norm as

$$\|A\|_{v_r, l} = \sum_{k=0}^{+\infty} \|\nabla_l^k(A)\|_2 / \{(k!)\}^r,$$

$$\|A\|_{c_r} = \left\{ \sum_{k \in \mathbb{Z}^d} \sup_{w_i, w_j \in \mathcal{D}} (A[i, j])^2 (1 + \|w_i - w_j\|_\infty)^{2r} \mathbb{1}_{\{w_i - w_j \in [0, 1)^{d+k}\}} \right\}^{1/2},$$

which are related to the functions v_r and c_r defined above. These two matrix norms describe the spatial decaying properties in the sense that if a matrix A has a finite $\|\cdot\|_{v_r, l}$ norm (or $\|\cdot\|_{c_r}$ norm), then its (i, j) -entry decays at the rate $1/v_r(\|w_i - w_j\|_\infty)$ (or $1/c_r(\|w_i - w_j\|_\infty)$). The following lemma is based on the work of Gröchenig and Klotz (2014) and Fang and Shin (2020).

LEMMA S4. *Let $A \in n \times n$ be an invertible matrix. If $\|A\|_{v_r, l} < \infty$ for some $r > 1$ and all $1 \leq l \leq d$, then*

$$\|A^{-1}\|_{v_r, l} \leq \|A^{-1}\|_2 v_{r-1}(\|A^{-1}\|_2 \|A\|_{v_r, l}).$$

If $\|\cdot\|_{c_r} < \infty$ for some $r \geq d + 1$, then there exist positive constants c_4, c_5 only dependent on the dimension d , such that

$$\|A^{-1}\|_{c_r} \leq c_4 c_5^r \{\max(1, 1/q)\}^{6d} \|A^{-1}\|_2 (\|A^{-1}\|_2 \|A\|_{c_r})^{r+d/2}.$$

Proof. PART 1 We prove the inequality for $\|\cdot\|_{v_r, l}$ norm. The idea is to first prove the bound holds if A is an infinite matrix using the theory of norm-controlled inversion, and then embed a finite-dimensional matrix into an infinite matrix.

Let $A \in \mathbb{R}^{\mathbb{Z} \times \mathbb{Z}}$ be an infinite matrix with finite $\|\cdot\|_{v_r, l}$ norm. We have two basic facts:

- (1) the collection of matrices of $\mathbb{R}^{\mathbb{Z} \times \mathbb{Z}}$ with finite matrix L_2 norm forms an algebra with matrix addition and multiplication as algebra addition and multiplication;
- (2) ∇_l is a differential operator on the algebra of matrices with finite L_2 norm.

Thus we can apply the norm-controlled inversion theory in Section 2.4 of Gröchenig and Klotz (2014) to bound the inversion A^{-1} . Specifically, let $B = A/\|A\|_{v_r, l}$ for some $r \geq 1$ and $l \in \mathbb{N}$, then applying equation (2.26) of Gröchenig and Klotz (2014) yields

$$\|B^{-1}\|_{v_r, l} \leq \|B^{-1}\|_2 v_{r-1}(\|B^{-1}\|_2).$$

Replacing $B^{-1} = \|A\|_{v_r, l} A^{-1}$, we have

$$\|A^{-1}\|_{v_r, l} \leq \|A^{-1}\|_2 v_{r-1}(\|A^{-1}\|_2 \|A\|_{v_r, l}).$$

Now consider the case when A is a finite matrix. Without loss of generality, we assume $\mathcal{I} = \{1, 2, \dots, n\}$ for $n \in \mathbb{N}$. Now expand \mathcal{I} into \mathbb{Z} by assigning each $i \in \mathbb{Z} \setminus \mathcal{I}$ a location $w_i \in \Omega$ such that for any $i, j \in \mathbb{Z}$ with $i \neq j$, $w_i \neq w_j$. We embed A into a matrix $\tilde{A} \in \mathbb{R}^{\mathbb{Z} \times \mathbb{Z}}$ such that

$$\tilde{A}[i, j] = \begin{cases} A[i, j], & i \in \mathcal{I} \text{ and } j \in \mathcal{I}, \\ \mathbb{1}_{\{i=j\}}, & i \notin \mathcal{I} \text{ or } j \notin \mathcal{I}. \end{cases}$$

Then again applying equation (2.26) of Gröchenig and Klotz (2014) on $\tilde{A}/\|\tilde{A}\|_{v_r, l}$, we similarly obtain

$$\|\tilde{A}^{-1}\|_{v_r, l} \leq \|\tilde{A}^{-1}\|_2 v_{r-1}(\|\tilde{A}^{-1}\|_2 \|\tilde{A}\|_{v_r, l}). \quad (\text{S6})$$

Since the matrix \tilde{A} can be represented as a block diagonal matrix

$$\tilde{A} = \begin{bmatrix} A & 0 \\ 0 & I_{\mathbb{Z} \setminus \mathcal{I}} \end{bmatrix}, \quad (\text{S7})$$

we have

$$\nabla_l^k(\tilde{A}) = \begin{bmatrix} \nabla_l^k(\tilde{A}) & 0 \\ 0 & I_{\mathbb{Z} \setminus \mathcal{I}} \end{bmatrix},$$

which implies that

$$\|\tilde{A}^{-1}\|_2 = \|A^{-1}\|_2, \quad \|\tilde{A}^{-1}\|_{v_r, l} = \|A^{-1}\|_{v_r, l}. \quad (\text{S8})$$

Combining equation (S8) with (S7), we obtain that

$$\|A^{-1}\|_{v_r, l} \leq \|A^{-1}\|_2 v_{r-1}(\|A^{-1}\|_2 \|A\|_{v_r, l}).$$

PART 2 We prove the inequality for $\|\cdot\|_{c_r, l}$ norm. Based on the same trick of part 1 that extends a finite matrix to an infinite matrix, Theorem 2 of Fang and Shin (2020) directly yields

$$\|A^{-1}\|_{c_r} \leq C \|A^{-1}\|_2 (\|A^{-1}\|_2 \|A\|_{c_r})^{r + \frac{d}{2}}, \quad (\text{S9})$$

for some positive constant C dependent on r, d and $R(\Lambda)$ in their paper. We only need to verify we can find C', C'' dependent on d , such that $C \leq C' C''^r (\max\{1, 1/q\})^6$. In the rest of the proof, we use $O(\cdot)$ to denote a quantity is no greater than some constants only dependent on d and r .

We first notice their $R(\Lambda)$ is the maximal number of locations in a cube $k + [0, 1)^d$. Thus we have

$$R(\Lambda) \leq \{\max(1, \lceil 1/q \rceil)\}^d = O(\{\max(1, 1/q)\}^d).$$

By the proof of their Proposition 1 (4), and our condition $r \geq d + 1$ in Lemma S4, their constant C_1 satisfies

$$C_1 = 2^{r+1} R(\Lambda) \left(\frac{3^d r}{r - d/2} \right)^{1/2} = O\left(2^r \{\max(1, 1/q)\}^d\right).$$

By the definition of $D_{d,p,r}$ in their proof of Theorem 2, we have

$$\begin{aligned} D_{d,p,r} &= 2^{3r+3} 11^{d+r} \{\max(1, 1/q)\}^d \left\{ \left(\frac{d}{2r-d} \right)^{1/2} + \left(\frac{d+2r}{2r-d-2} \right)^{1/2} \right\} \\ &= O(88^r \{\max(1, 1/q)\}^d). \end{aligned}$$

Finally, by their equations (42), (34) and (35), the constant C in (S9) satisfies that

$$\begin{aligned} C &\leq 10^{d/2+r+d+1} N_0^{d/p+r} \\ &= O\left(10^r (C_1 D_{d,p,r})^{\sup_{r \geq d+1} \frac{r+d/2}{\min\{1, r-d/2\}}}\right) \\ &= O\left(10^r (C_1 D_{d,p,r})^3\right) \\ &= O\left(10^r [(2 \times 88)^r \{\max(1, 1/q)\}^{2d}]^3\right) \\ &= O\left((10 \times 176^3)^r \{\max(1, 1/q)\}^{6d}\right). \end{aligned}$$

The conclusion of Lemma S4 follows from this upper bound on C and (S9). The constants computed above using the results in Fang and Shin (2020) are merely for the purpose of proving the existence of the constant C . In the literature of norm-controlled inversion, these constants are not carefully tuned and not tight in general. \square

S2.4. Bounds for $\max_i \|l_i - \hat{l}_i\|_2$ under Decaying Covariance Functions

We are finally ready to present upper bounds for $\max_i \|l_i - l\|_2$. The first result applies to the situation where the decay rate of the covariance function is no slower than $1/v_r$.

LEMMA S5. Suppose that $Z \in \mathcal{Z}_{v_r}$ for some $r > 1$. If $0 < q < 1$ and

$$\frac{n^{1/2}}{v_r(\rho d^{-1/2})} \{\phi_0(c_2/q)\}^{-9/2} v_{r-1}(c_3 \{\phi_0(c_2/q)\}^{-1}) \leq c_6$$

for some constant c_6 only dependent on d , then

$$\max_i \|l_i - \hat{l}_i\|_2 \lesssim \frac{1}{v_r(\rho d^{-1/2})} \{\phi_0(c_2/q)\}^{-\frac{9}{2}} q^{\frac{1}{2}d} v_{r-1}(c_3 \{\phi_0(c_2/q)\}^{-1}), \quad (\text{S10})$$

$$\text{and } \|\hat{\Phi} - \Sigma_{\mathcal{D}\mathcal{D}}^{-1}\|_2 \leq \frac{1}{2} \|\Sigma_{\mathcal{D}\mathcal{D}}^{-1}\|_2. \quad (\text{S11})$$

Else if $q \geq 1$ and $n^{1/2} \{v_r(\rho d^{-1/2})\}^{-1} \leq c'_6$ for some constant c'_6 only dependent on d , then equation (S11) still holds, and

$$\max_i \|l_i - \hat{l}_i\|_2 \lesssim \frac{1}{v_r(\rho d^{-1/2})}. \quad (\text{S12})$$

Proof. PART 1 We first prove the upper bounds for $\max_i \|l - \hat{l}\|_2$ for both the cases of $0 < q < 1$ and $q \geq 1$. Fix an arbitrary $i \in \{1, 2, \dots, n\}$. For simplicity of notation, define the sets N and O as

$$N = \{w_j \in \mathcal{D} : j < i, \|w_i - w_j\|_2 < \rho\},$$

$$O = \{w_j \in \mathcal{D} : j < i, \|w_i - w_j\|_2 \geq \rho\}.$$

With a little abuse of notation, we denote the i th column of matrix $I_n - B^T$ and $I_n - \hat{B}^T$ as b_i and \hat{b}_i ; denote Φ_{NN} as the submatrix of $(\Sigma[\nu(i), \nu(i)])^{-1}$ whose rows and columns correspond to set N ; similarly define Φ_{ON} , Φ_{NO} and Φ_{OO} . In the rest of the proof, we reorder the indices of elements in the sets N and O such that the indices of elements in N are always smaller than those in O . In this way, we are able to formulate various computations as block matrix computations. By the definition of Φ_{NN} and Φ_{ON} , we have

$$\Sigma_{NN}\Phi_{NN} + \Sigma_{NO}\Phi_{ON} = I_N.$$

Thus

$$\Phi_{NN} = \Sigma_{NN}^{-1} - \Sigma_{NN}^{-1}\Sigma_{NO}\Phi_{ON}.$$

We can formulate b_i and \hat{b}_i as

$$b_i = \begin{bmatrix} 1 \\ \Phi_{NN}\Sigma_{N,w_i} + \Phi_{NO}\Sigma_{O,w_i} \\ \Phi_{ON}\Sigma_{N,w_i} + \Phi_{OO}\Sigma_{O,w_i} \end{bmatrix}, \quad \hat{b}_i = \begin{bmatrix} 1 \\ \Sigma_{NN}^{-1}\Sigma_{N,w_i} \\ 0 \end{bmatrix}.$$

Therefore we have

$$\begin{aligned} \|b_i - \hat{b}_i\|_2 &\leq \|(\Phi_{NN} - \Sigma_{NN}^{-1})\Sigma_{N,w_i} + \Phi_{NO}\Sigma_{O,w_i}\|_2 + \|\Phi_{ON}\Sigma_{N,w_i} + \Phi_{OO}\Sigma_{O,w_i}\|_2 \\ &\leq \|-\Sigma_{NN}^{-1}\Sigma_{NO}\Phi_{ON}\Sigma_{N,w_i}\|_2 + \|\Phi_{NO}\Sigma_{O,w_i}\|_2 + \|\Phi_{ON}\Sigma_{N,w_i}\|_2 + \|\Phi_{OO}\Sigma_{O,w_i}\|_2. \end{aligned} \quad (\text{S13})$$

Similarly, for $D[i, i]$ and $\hat{D}[i, i]$, we have

$$D[i, i] = \Sigma_{w_i, w_i} - \Sigma_{N, w_i}^T \Phi_{NN} \Sigma_{N, w_i} - 2\Sigma_{N, w_i}^T \Phi_{NO} \Sigma_{O, w_i} - \Sigma_{O, w_i}^T \Phi_{OO} \Sigma_{O, w_i},$$

$$\hat{D}[i, i] = \Sigma_{w_i, w_i} - \Sigma_{N, w_i}^T \Sigma_{NN}^{-1} \Sigma_{N, w_i}.$$

Thus

$$\begin{aligned} |D[i, i] - \hat{D}[i, i]| &\leq -\Sigma_{N, w_i}^T (\Phi_{NN} - \Sigma_{NN}^{-1}) \Sigma_{N, w_i} - 2\Sigma_{N, w_i}^T \Phi_{NO} \Sigma_{O, w_i} - \Sigma_{O, w_i}^T \Phi_{OO} \Sigma_{O, w_i} \\ &\leq |\Sigma_{N, w_i}^T \Sigma_{NN}^{-1} \Sigma_{NO} \Phi_{ON} \Sigma_{N, w_i}| + 2|\Sigma_{N, w_i}^T \Phi_{NO} \Sigma_{O, w_i}| + |\Sigma_{O, w_i}^T \Phi_{OO} \Sigma_{O, w_i}|. \end{aligned} \quad (\text{S14})$$

The term $\Phi_{ON}\Sigma_{N, w_i}$ appears multiple times in bounds (S13) and (S14). The next technical lemma shows it can be controlled by approximation radius ρ .

Technical Lemma S2. For the submatrices Φ_{ON} and Σ_{N, w_i} defined above, we have

$$\|\Phi_{ON}\Sigma_{N, w_i}\|_2 \leq \frac{1}{v_r(\rho d^{-1/2})} c_3 \{\phi_0(c_2/q)\}^{-1} v_{r-1}(c_3 \{\phi_0(c_2/q)\}^{-1}).$$

Proof. Applying Lemma S4 to the matrix $\Sigma_{\nu(i), \nu(i)}$, we have that for any $l \in \mathbb{N}$,

$$\begin{aligned} \|\Phi_{ON}\|_{v_r, l} &\leq \|(\Sigma[\nu(i), \nu(i)])^{-1}\|_{v_r, l} \\ &\leq \|(\Sigma[\nu(i), \nu(i)])^{-1}\|_2 v_{r-1} (\|(\Sigma[\nu(i), \nu(i)])^{-1}\|_2 \|(\Sigma[\nu(i), \nu(i)])\|_{v_r, l}) \\ &\leq \|\Sigma_{\mathcal{DD}}^{-1}\|_2 v_{r-1} (\|\Sigma_{\mathcal{DD}}^{-1}\|_2 \|\Sigma_{\mathcal{DD}}\|_{v_r, l}) \\ &\leq c_1 \{\phi_0(c_2/q)\}^{-1} q^d v_{r-1} \left(c_1 \{\phi_0(c_2/q)\}^{-1} 2^d (1 + q/2)^{d-1} (1 + q/2 + d) \right), \end{aligned} \quad (\text{S15})$$

where the last step follows from Lemma S2.

Now define a matrix operator $\tilde{\nabla}$ such that for all $A \in \mathbb{R}^{\mathcal{I} \times \mathcal{I}}$, $\tilde{\nabla}(A) \in \mathbb{R}^{\mathcal{I} \times \mathcal{I}}$ has its (i, j) -entry defined as

$$\tilde{\nabla}(A)[i, j] = v_r(\|w_i - w_j\|_2 / d^{1/2}) A[i, j].$$

Since for all $w_i, w_j \in \mathcal{D}$, $\sup_{1 \leq l \leq d} |w_i[l] - w_j[l]| \geq \|w_i - w_j\|_2 / d^{1/2}$, we have that for the column of Φ_{ON} corresponding to $w_k \in N$,

$$\begin{aligned} \|\tilde{\nabla}\Phi_{O, w_k}\|_2 &= \left[\sum_{w_j \in O} \{v_r(\|w_i - w_j\|_2 / d^{1/2}) \Phi_{w_j, w_k}\}^2 \right]^{1/2} \\ &\leq \left[\sum_{w_j \in O} \left\{ \sup_{1 \leq l \leq d} v_r(|w_i[l] - w_j[l]|) \Phi_{w_j, w_k} \right\}^2 \right]^{1/2} \end{aligned}$$

$$\begin{aligned}
&\leq \left[\sum_{w_j \in O} \left\{ \sum_{l=1}^d v_r(|w_i[l] - w_j[l]|) \Phi_{w_j, w_k} \right\}^2 \right]^{1/2} \\
&\leq \sum_{l=1}^d \left[\sum_{w_j \in O} \{v_r(|w_i[l] - w_j[l]|) \Phi_{w_j, w_k}\}^2 \right]^{1/2} \\
&\leq \sum_{1 \leq l \leq d} \|\Phi_{O, w_k}\|_{v_r, l} \leq \sum_{1 \leq l \leq d} \|\Phi_{ON}\|_{v_r, l} \\
&\leq dc_1 \{\phi_0(c_2/q)\}^{-1} q^d v_{r-1} \left(c_1 \{\phi_0(c_2/q)\}^{-1} 2^d (1 + q/2)^{d-1} (1 + d + q/2) \right),
\end{aligned}$$

where the last inequality follows from (S15).

Therefore, when $Z \in \mathcal{Z}_{v_r}$, we can derive that

$$\begin{aligned}
\|\Phi_{ON} \Sigma_{N, w_i}\|_2 &\leq \sum_{w_k \in N} \|\Phi_{O, w_k}\|_2 K_0(w_k, w_i) \\
&\leq \sum_{w_k \in N} \|\tilde{\nabla} \Phi_{O, w_k}\|_2 \frac{1}{\inf_{w_j \in O} v_r(\|w_j - w_k\|_2 d^{-1/2})} \\
&\quad \times \frac{1}{v_r(\|w_k - w_i\|_2) (1 + \|w_k - w_i\|_2^{d+1})} \\
&\leq \sum_{w_k \in N} \|\tilde{\nabla} \Phi_{O, w_k}\|_2 \frac{1}{\inf_{w_j \in O} v_r(\|w_j - w_i\|_2 d^{-1/2})} \frac{1}{1 + \|w_k - w_i\|_2^{d+1}} \\
&\leq \sum_{w_k \in N} \|\tilde{\nabla} \Phi_{O, w_k}\|_2 \frac{1}{v_r(\rho d^{-1/2})} \frac{1}{1 + \|w_k - w_i\|_2^{d+1}} \\
&\leq \frac{1}{v_r(\rho d^{-1/2})} d 2^d q^{-d} (1 + q/2)^{d-1} (1 + d + q/2) \cdot dc_1 \{\phi_0(c_2/q)\}^{-1} q^d \\
&\quad \times v_{r-1} \left(c_1 \{\phi_0(c_2/q)\}^{-1} 2^d (1 + q/2)^{d-1} (1 + d + q/2) \right) \\
&\leq \frac{1}{v_r(\rho d^{-1/2})} c_3 \{\phi_0(c_2/q)\}^{-1} v_{r-1} (c_3 \{\phi_0(c_2/q)\}^{-1}).
\end{aligned}$$

where $c_3 = c_1 d^2 2^d (1 + d + q/2) (1 + q/2)^{d-1}$, and the third inequality is due to the fact that v_r is submultiplicative. When $q < 1$, c_3 can be regarded as a constant independent of q . \square

We now come back to the proof of the main Lemma S5 and first consider the situation where $q < 1$. The elements of the column vector Σ_{O, w_i} are the covariances between locations that are at least ρ distance apart. Therefore, we have

$$\begin{aligned}
\|\Sigma_{O, w_i}\|_2 &\leq \sum_{j=1}^n K(w_i, w_j) \mathbb{1}_{\{\|w_i - w_j\|_2 \geq \rho\}} \\
&\leq \sum_{j=1}^n \frac{1}{v_r(\rho)} \frac{1}{1 + \|w_i - w_j\|_2^{d+1}} \mathbb{1}_{\{\|w_i - w_j\|_2 \geq \rho\}} \\
&\leq \frac{\Gamma(d/2 + 1) 2^d}{\pi^{d/2} q^d} \frac{1}{v_r(\rho)} \int_{\rho - q/2}^{+\infty} \frac{2\pi^{d/2} x^{d-1}}{\Gamma(d/2)} \frac{1}{1 + (x - q/2)^{d+1}} dx
\end{aligned}$$

$$\leq \frac{\pi d 2^{d-1} q^{-d}}{v_r(\rho)}. \quad (\text{S16})$$

Using Technical Lemma S2 and equation (S16) while controlling all other terms in $\|b_i - \hat{b}_i\|$ and $|D[i, i] - \hat{D}[i, i]|$ with the matrix l_2 norm, we have that

$$\begin{aligned} \|b_i - \hat{b}_i\|_2 &\leq (\|\Sigma_{\mathcal{DD}}\|_2 \|\Sigma_{\mathcal{DD}}^{-1}\|_2 + 1) \|\Phi_{ON} \Sigma_{N, w_i}\|_2 + 2 \|\Sigma_{\mathcal{DD}}^{-1}\|_2 \|\Sigma_{O, w_i}\|_2 \\ &\lesssim \frac{1}{v_r(\rho d^{-1/2})} q^{-d} \{\phi_0(c_2/q)\}^{-1} q^d c_3 \{\phi_0(c_2/q)\}^{-1} v_{r-1}(c_3 \{\phi_0(c_2/q)\}^{-1}) \\ &\quad + \{\phi_0(c_2/q)\}^{-1} q^d q^{-d} v_r(\rho)^{-1} \\ &\lesssim \frac{1}{v_r(\rho d^{-1/2})} \{\phi_0(c_2/q)\}^{-2} v_{r-1}(c_3 \{\phi_0(c_2/q)\}^{-1}), \end{aligned} \quad (\text{S17})$$

$$\begin{aligned} |D[i, i] - \hat{D}[i, i]| &\leq \|\Sigma_{\mathcal{DD}}\|_2^2 \|\Sigma_{\mathcal{DD}}^{-1}\|_2 \|\Phi_{ON} \Sigma_{N, w_i}\|_2 + (\|\Sigma_{\mathcal{DD}}\|_2 + 1) \|\Sigma_{\mathcal{DD}}^{-1}\|_2 \|\Sigma_{O, w_i}\|_2 \\ &\lesssim \frac{1}{v_r(\rho d^{-1/2})} q^{-2d} \{\phi_0(c_2/q)\}^{-1} q^d c_3 \{\phi_0(c_2/q)\}^{-1} v_{r-1}(c_3 \{\phi_0(c_2/q)\}^{-1}) \\ &\quad + q^{-d} \{\phi_0(c_2/q)\}^{-1} q^d v_r(\rho)^{-1} \\ &\lesssim \frac{1}{v_r(\rho d^{-1/2})} \{\phi_0(c_2/q)\}^{-2} q^{-d} v_{r-1}(c_3 \{\phi_0(c_2/q)\}^{-1}), \end{aligned} \quad (\text{S18})$$

where the multiplicative constants under the \lesssim relations only depend on d . We also have the following bounds for b_i , $(D[i, i])^{-1}$ and $(\hat{D}[i, i])^{-1}$:

$$\begin{aligned} \|b_i\|_2 &= \|(\Sigma[\nu(i), \nu(i)])^{-1} \Sigma[\nu(i), i]\|_2 \lesssim \{\phi_0(c_2/q)\}^{-1}, \\ \min \{(D[i, i])^{-1}, (\hat{D}[i, i])^{-1}\} &\geq K(w_i, w_i)^{-1} = 1/K_0(0), \\ (D[i, i])^{-1} &\leq \|(\Sigma[\nu(i), \nu(i)])^{-1}\|_2 \lesssim \{\phi_0(c_2/q)\}^{-1} q^d, \\ (\hat{D}[i, i])^{-1} &\leq \|(\Sigma_{N \cup \{w_i\}, N \cup \{w_i\}})^{-1}\|_2 \lesssim \{\phi_0(c_2/q)\}^{-1} q^d. \end{aligned} \quad (\text{S19})$$

Combining equations (S17) to (S19), when $q < 1$, we can bound $\|l_i - \hat{l}_i\|_2$ as

$$\begin{aligned} &\|l_i - \hat{l}_i\|_2 \\ &= \|b_i(D[i, i])^{-1/2} - \hat{b}_i(\hat{D}[i, i])^{-1/2}\|_2 \\ &\leq \|b_i\|_2 |(D[i, i])^{-1/2} - (\hat{D}[i, i])^{-1/2}| + \|b_i - \hat{b}_i\|_2 (D[i, i])^{-1/2} \\ &\quad + \|b_i - \hat{b}_i\|_2 |(D[i, i])^{-1/2} - (\hat{D}[i, i])^{-1/2}| \\ &\lesssim \|b_i\|_2 \left([\{\phi_0(c_2/q)\}^{-1} q^d]^{3/2} |D[i, i] - \hat{D}[i, i]| \right. \\ &\quad \left. + [\{\phi_0(c_2/q)\}^{-1} q^d]^{5/2} O((D[i, i] - \hat{D}[i, i])^2) \right) \\ &\quad + \|b_i - \hat{b}_i\|_2 (D[i, i])^{-1/2} \\ &\quad + \|b_i - \hat{b}_i\|_2 \left([\{\phi_0(c_2/q)\}^{-1} q^d]^{3/2} |D[i, i] - \hat{D}[i, i]| \right. \\ &\quad \left. + [\{\phi_0(c_2/q)\}^{-1} q^d]^{5/2} O((D[i, i] - \hat{D}[i, i])^2) \right) \\ &\lesssim \frac{1}{v_r(\rho d^{-1/2})} \{\phi_0(c_2/q)\}^{-9/2} q^{1/2} d v_{r-1}(c_3 \{\phi_0(c_2/q)\}^{-1}) \end{aligned}$$

$$\begin{aligned}
& + \frac{1}{v_r(\rho d^{-1/2})} \{\phi_0(c_2/q)\}^{-\frac{5}{2}} q^{\frac{1}{2}d} v_{r-1}(c_3 \{\phi_0(c_2/q)\}^{-1}) \\
& \lesssim \frac{1}{v_r(\rho d^{-1/2})} \{\phi_0(c_2/q)\}^{-\frac{9}{2}} q^{\frac{1}{2}d} v_{r-1}(c_3 \{\phi_0(c_2/q)\}^{-1}).
\end{aligned}$$

This completes the proof of (S10).

If $q \geq 1$, both the minimal and maximal eigenvalues of $\Sigma_{\mathcal{DD}}$ are bounded by constants by (S19). Therefore, all terms involving q in (S10) become constant and we have

$$\|l_i - \hat{l}_i\|_2 \lesssim \frac{1}{v_r(\rho d^{-1/2})}.$$

Since the above arguments hold for arbitrary i , we finish the proof of (S12).

PART 2 We now derive a sufficient condition for $\|\hat{L} - L\|_2 \leq \|\Sigma_{\mathcal{DD}}\|_2^{-1/2}/2$. The left hand side can be bounded as

$$\|\hat{L} - L\|_2 \leq n^{1/2} \max_i \|\hat{l}_i - l_i\|_2.$$

We first consider the case $0 < q < 1$. A sufficient condition for $\|\hat{L} - L\|_2 \leq \|\Sigma_{\mathcal{DD}}\|_2^{-1/2}/2$ is

$$2\|\Sigma_{\mathcal{DD}}\|_2^{1/2} n^{1/2} \max_i \|\hat{l}_i - l_i\|_2 \leq 1. \quad (\text{S20})$$

By applying Lemma S2 and part 1 of this proof to equation (S20), we get the following sufficient condition

$$\frac{n^{1/2}}{v_r(\rho d^{-1/2})} \{\phi_0(c_2/q)\}^{-9/2} v_{r-1}(c_3 \{\phi_0(c_2/q)\}^{-1}) \leq c_6, \quad (\text{S21})$$

for some constant c_6 only dependent on d .

Now for the case $q > 1$, all terms involving q can be considered as constants, leaving n and ρ as the only variables. Therefore, a sufficient condition for $\|\hat{L} - L\|_2 \leq \|\Sigma_{\mathcal{DD}}\|_2^{-1/2}/2$ is $n^{1/2} \{v_r(\rho d^{-1/2})\}^{-1} \leq c'_6$ for some constant c'_6 only dependent on d . \square

For the polynomial decaying class \mathcal{Z}_{c_r} , we have a similar result.

LEMMA S6. Suppose that $Z \in \mathcal{Z}_{c_r}$ for some $r \geq d + 1$. If $0 < q < 1$ and

$$\frac{n^{1/2}}{(1 + \rho d^{-1/2})^{r-d-1}} q^{(r-7)d} \{\phi_0(c_2/q)\}^{-(r+4)} (c_1 c_5 d 2^{d-1} \pi / \sqrt{6})^r \leq c_7$$

for some constant c_7 only dependent on d , then equation (S11) holds and

$$\|l_i - \hat{l}_i\|_2 \lesssim \frac{1}{(1 + \rho d^{-1/2})^{r-d-1}} q^{(r-13/2)d} \{\phi_0(c_2/q)\}^{-(r+4)} (c_1 c_5 d 2^{d-1} \pi / \sqrt{6})^r.$$

Else if $q \geq 1$ and $n^{1/2} (1 + \rho d^{-1/2})^{-(r-d-1)} \{\phi_0(c_2/q)\}^{-r} (c_1 c_5 d 2^{d-1} \pi / \sqrt{6})^r \leq c'_7$ for some constant c'_7 only dependent on d , then equation (S11) still holds and

$$\|l_i - \hat{l}_i\|_2 \lesssim \frac{1}{(1 + \rho d^{-1/2})^{r-d-1}} \{\phi_0(c_2/q)\}^{-r} \{c_1 c_5 d 2^{d-1} \pi / \sqrt{6}\}^r.$$

Proof. **PART 1** We first prove the upper bounds for $\max_i \|l - \hat{l}\|_2$. The proof is the same as that of Lemma S5 till equation (S14). We begin with the bounds on $\|\Sigma_{O,w_i}\|_2$ and $\|\Phi_{ON}\Sigma_{N,w_i}\|_2$.

$$\begin{aligned}
\|\Sigma_{O,w_i}\|_2 &\leq \left[\sum_{j=1}^n \{K(w_i, w_j)\}^2 \mathbb{1}_{\{\|w_i - w_j\|_2 \geq \rho\}} \right]^{1/2} \\
&\leq \left[\sum_{j=1}^n \frac{1}{(1 + \|w_i - w_j\|_2)^{2r}} \mathbb{1}_{\{\|w_i - w_j\|_2 \geq \rho\}} \right]^{1/2} \\
&\leq \frac{1}{(1 + \rho)^{r-(d+1)/2}} \left[\sum_{j=1}^n \frac{1}{(1 + \|w_i - w_j\|_2)^{d+1}} \mathbb{1}_{\{\|w_i - w_j\|_2 \geq \rho\}} \right]^{1/2} \\
&\leq \frac{1}{(1 + \rho)^{r-(d+1)/2}} \left[\frac{\Gamma(d/2 + 1)2^d}{\pi^{d/2}q^d} \int_{\rho-q/2}^{+\infty} \frac{2\pi^{d/2}x^{d-1}}{\Gamma(d/2)} \frac{1}{1 + (x - q/2)^{d+1}} dx \right]^{1/2} \\
&\leq \frac{(\pi d 2^{d-1} q^{-d})^{1/2}}{(1 + \rho)^{r-(d+1)/2}}.
\end{aligned}$$

To bound $\|\Phi_{ON}\Sigma_{N,w_i}\|_2$, we first consider the norm for columns of $\|\Phi_{ON}\|_2$. Define an operator $c_r \odot$ such that for any matrix $A \in \mathbb{R}^{\mathcal{I} \times \mathcal{I}}$, $c \odot A \in \mathbb{R}^{\mathcal{I} \times \mathcal{I}}$ has its (i, j) -entry defined as

$$c \odot A[i, j] = (1 + \|w_i - w_j\|_2 d^{-1/2})^{r-(d+1)/2} A[i, j].$$

Since for all $w_i, w_j \in \mathcal{D}$, $\|w_i - w_j\|_\infty \geq \|w_i - w_j\|_2 d^{-1/2}$, we have for all $w_k \in N$, for the column of Φ_{ON} corresponding to $w_k \in N$,

$$\begin{aligned}
\|c \odot \Phi_{O,w_k}\|_2 &\leq [\max\{1, \lceil 1/q \rceil\}]^{d/2} \|\Phi_{O,w_k}\|_{r-(d+1)/2} \\
&\leq [\max\{1, \lceil 1/q \rceil\}]^{d/2} \|(\Sigma[\nu(i), \nu(i)])^{-1}\|_{r-(d+1)/2} \\
&\stackrel{(i)}{\leq} [\max\{1, \lceil 1/q \rceil\}]^{\frac{13}{2}d} c_4 c_5^{r-(d+1)/2} \|(\Sigma[\nu(i), \nu(i)])^{-1}\|_2 \\
&\quad \{ \|(\Sigma[\nu(i), \nu(i)])^{-1}\|_2 \|(\Sigma[\nu(i), \nu(i)])\|_{c_{r-(d+1)/2}} \}^{r-1/2} \\
&\leq [\max\{1, \lceil 1/q \rceil\}]^{\frac{13}{2}d} c_4 c_5^{r-(d+1)/2} \|\Sigma_{\mathcal{DD}}^{-1}\|_2 (\|\Sigma_{\mathcal{DD}}^{-1}\|_2 \|\Sigma_{\mathcal{DD}}\|_{c_{r-(d+1)/2}})^{r-1/2} \\
&\stackrel{(ii)}{\leq} c_4 c_5^{r-(d+1)/2} [\max\{1, \lceil 1/q \rceil\}]^{\frac{13}{2}d} [c_1 \{\phi_0(c_2/q)\}^{-1} q^d]^{r+1/2} (d 2^{d-1} \pi / \sqrt{6})^{r-1/2},
\end{aligned}$$

where (i) follows from Lemma S4, and (ii) follows from (5) of Lemma S2.

We first consider the case $q < 1$. We have

$$\|c \odot \Phi_{O,w_k}\|_2 \lesssim q^{(r-6)d} \{\phi_0(c_2/q)\}^{-(r+1/2)} (c_1 c_5 d 2^{d-1} \pi / \sqrt{6})^r,$$

where the constant in \lesssim is only dependent on d . Therefore we have

$$\begin{aligned}
&\|\Phi_{ON}\Sigma_{N,w_i}\|_2 \\
&\leq \sum_{w_k \in N} \|\Phi_{O,w_k}\|_2 K_0(w_k, w_i) \\
&\leq \sum_{w_k \in N} \|c \odot \Phi_{O,w_k}\|_2 \frac{1}{\inf_{w_j \in O} (1 + \|w_j - w_k\|_2 d^{-1/2})^{r-(d+1)/2}} \frac{1}{(1 + \|w_i - w_k\|_2)^r}
\end{aligned}$$

$$\begin{aligned}
&\leq \sum_{w_k \in N} \|c \odot \Phi_{O, w_k}\|_2 \frac{1}{\inf_{w_j \in O} (1 + \|w_j - w_k\|_2 d^{-1/2} + \|w_i - w_k\|_2)^{r-(d+1)/2}} \\
&\quad \times \frac{1}{(1 + \|w_i - w_k\|_2)^{(d+1)/2}} \\
&\leq \sum_{w_k \in N} \|c \odot \Phi_{O, w_k}\|_2 \frac{1}{(1 + \rho d^{-1/2} + \|w_i - w_k\|_2)^{r-(d+1)/2}} \frac{1}{(1 + \|w_i - w_k\|_2)^{(d+1)/2}} \\
&\leq \sum_{w_k \in N} \|c \odot \Phi_{O, w_k}\|_2 \frac{1}{(1 + \rho d^{-1/2})^{r-d-1}} \frac{1}{(1 + \|w_i - w_k\|_2)^{d+1}} \\
&\leq \pi d 2^{d-1} q^{-d} \sup_{w_k \in N} \|c \odot \Phi_{O, w_k}\|_2 \frac{1}{(1 + \rho d^{-1/2})^{r-d-1}} \\
&\lesssim \frac{1}{(1 + \rho d^{-1/2})^{r-d-1}} q^{-d} q^{(r-6)d} \{\phi_0(c_2/q)\}^{-(r+1/2)} (c_1 c_5 d 2^{d-1} \pi / \sqrt{6})^r \\
&\lesssim \frac{1}{(1 + \rho d^{-1/2})^{r-d-1}} q^{(r-7)d} \{\phi_0(c_2/q)\}^{-(r+1/2)} (c_1 c_5 d 2^{d-1} \pi / \sqrt{6})^r.
\end{aligned}$$

The rest of the proof follows a similar strategy as that of Lemma S5. We now only list the key steps.

$$\begin{aligned}
\|b_i - \hat{b}_i\|_2 &\leq (\|\Sigma_{\mathcal{DD}}\|_2 \|\Sigma_{\mathcal{DD}}^{-1}\|_2 + 1) \|\Phi_{ON} \Sigma_{N, w_i}\|_2 + 2 \|\Sigma_{\mathcal{DD}}^{-1}\|_2 \|\Sigma_{O, w_i}\|_2 \\
&\lesssim \frac{1}{(1 + \rho d^{-1/2})^{r-d-1}} q^{(r-7)d} \{\phi_0(c_2/q)\}^{-(r+3/2)} (c_1 c_5 d 2^{d-1} \pi / \sqrt{6})^r, \\
|D[i, i] - \hat{D}[i, i]| &\leq \|\Sigma_{\mathcal{DD}}\|_2^2 \|\Sigma_{\mathcal{DD}}^{-1}\|_2 \|\Phi_{ON} \Sigma_{N, w_i}\|_2 + (\|\Sigma_{\mathcal{DD}}\|_2 + 1) \|\Sigma_{\mathcal{DD}}^{-1}\|_2 \|\Sigma_{O, w_i}\|_2 \\
&\lesssim \frac{1}{(1 + \rho d^{-1/2})^{r-d-1}} q^{(r-8)d} \{\phi_0(c_2/q)\}^{-(r+3/2)} (c_1 c_5 d 2^{d-1} \pi / \sqrt{6})^r. \\
\|l_i - \hat{l}_i\|_2 &\leq \|b\|_2 |(D[i, i])^{-1/2} - (\hat{D}[i, i])^{-1/2}| + \|b_2 - \hat{b}_2\|_2 (D[i, i])^{-1/2} \\
&\quad + \|b_2 - \hat{b}_2\|_2 |(\hat{D}[i, i])^{-1/2} - (D[i, i])^{-1/2}| \\
&\lesssim \frac{1}{(1 + \rho d^{-1/2})^{r-d-1}} q^{(r-13/2)d} \{\phi_0(c_2/q)\}^{-(r+4)} (c_1 c_5 d 2^{d-1} \pi / \sqrt{6})^r.
\end{aligned}$$

If $q \geq 1$, then we have a simplified bound as

$$\|l_i - \hat{l}_i\|_2 \lesssim \frac{1}{(1 + \rho d^{-1/2})^{r-d-1}} \{\phi_0(c_2/q)\}^{-r} (c_1 c_5 d 2^{d-1} \pi / \sqrt{6})^r.$$

PART 2 A sufficient condition for $\|\hat{L} - L\|_2 \leq \|\Sigma_{\mathcal{DD}}\|_2^{-1/2}/2$ can be derived by satisfying equation (S20) in the proof of Lemma S5. When $q < 1$, this yields

$$\frac{n^{1/2}}{(1 + \rho d^{-1/2})^{r-d-1}} q^{(r-7)d} \{\phi_0(c_2/q)\}^{-(r+4)} (c_1 c_5 d 2^{d-1} \pi / \sqrt{6})^r \leq c_7$$

for some constant c_7 only dependent on d . When $q \geq 1$, this yields

$$\frac{n^{1/2}}{(1 + \rho d^{-1/2})^{r-d-1}} \{\phi_0(c_2/q)\}^{-r} (c_1 c_5 d 2^{d-1} \pi / \sqrt{6})^r \leq c'_7$$

for some constant c'_7 only dependent on d . \square

S3. PROOF OF THEOREMS AND COROLLARY IN SECTION 3 OF THE MAIN TEXT

S3.1. Proof of Theorems 1 and 2

Proof of Theorem 1. We first consider the case $0 < q < 1$. Since the second term in Lemma S1 of the main text is dominated by the first term as shown in the proof of Lemma S5, we plug the results of Lemmas S2 and S5 into Lemma S1 to obtain that

$$\begin{aligned} & W_2^2(Z_{\mathcal{D}}, \hat{Z}_{\mathcal{D}}) \\ & \lesssim n \|\Sigma_{\mathcal{D}\mathcal{D}}\|_2^2 (\|\Sigma_{\mathcal{D}\mathcal{D}}^{-1}\|_2)^{-1/2} \max_i \|l_i - \hat{l}_i\|_2 \\ & \lesssim q^{-2d} \{\phi_0(c_2/q)\}^{-\frac{1}{2}} q^{\frac{d}{2}} \cdot \frac{1}{v_r(\rho d^{-1/2})} \{\phi_0(c_2/q)\}^{-\frac{9}{2}} q^{\frac{1}{2}d} v_{r-1}(c_3 \{\phi_0(c_2/q)\}^{-1}) \\ & \lesssim \frac{n}{v_r(\rho d^{-1/2})} \{\phi_0(c_2/q)\}^{-5} q^{-d} v_{r-1}(c_3 \{\phi_0(c_2/q)\}^{-1}). \end{aligned}$$

For the case when $q \geq 1$, all terms involving q can be considered as constants, thus we have

$$W_2^2(Z_{\mathcal{D}}, \hat{Z}_{\mathcal{D}}) \lesssim \frac{n}{v_r(\rho d^{-1/2})}.$$

Since the above results hold for all $Z \in \mathcal{Z}_{v_r}$, we finish the proof of Theorem 1. \square

The proof of Theorem 2 follows the same steps as the proof of Theorem 1, with Lemma S5 replaced by Lemma S6.

S3.2. Proof of Corollary 1

We first prove a technical lemma.

Technical Lemma S3. For all $x > 0$, we have

$$v_2(x^3) \geq \{v_1(x)\}^3.$$

Proof.

$$\begin{aligned} v_2(x^3) &= \sum_{k=0}^{\infty} \frac{x^{3k}}{(k!)^{3/2}} \frac{1}{(k!)^{1/2}} \\ &= \sum_{j=0}^{\infty} \frac{1}{(j!)^{1/2}} \sum_{k=0}^{\infty} \left\{ \frac{x^k}{(k!)^{1/2}} \right\}^3 \frac{\frac{1}{(k!)^{1/2}}}{\sum_{j=0}^{\infty} \frac{1}{(j!)^{1/2}}} \\ &\stackrel{\text{Jensen}}{\geq} \sum_{j=0}^{\infty} \frac{1}{(j!)^{1/2}} \left\{ \sum_{k=0}^{\infty} \frac{x^k}{(k!)^{1/2}} \frac{1}{(k!)^{1/2}} \right\}^3 \\ &\geq [v_1(x)]^3. \end{aligned}$$

\square

Proof. We now prove the results for the three covariance functions.

MATÉRN Let $r = 2$. Since the Matérn covariance function decays at the rate $K_0(\|s_1 - s_2\|_2) = O(\|s_1 - s_2\|_2^{\nu-1/2} \exp(-\phi\|s_1 - s_2\|_2)) \lesssim v_2(\phi\|s_1 - s_2\|_2)$, we have $Z \in \mathcal{Z}_{v_2}$ up to a

scale parameter ϕ . Thus when $q < 1/\phi$, Theorem 1 in the main paper gives

$$W_2^2(Z_D, \hat{Z}_D) \lesssim \frac{1}{v_2(\phi \rho d^{-1/2})} \exp \left(c_3 \{ \phi_0(c_2/(\phi q)) \}^{-1} + \ln \left[n q^{-d} \{ \phi_0(c_2/(\phi q)) \}^{-5} \right] \right), \quad (\text{S22})$$

where $\phi_0(\cdot)$ is the Fourier transform of Matérn covariance function with scale parameter $\phi = 1$, which has the closed form solution

$$\hat{K}_0(\xi) = \frac{\tau^2 2^d \pi^{d/2} \Gamma(\nu + d/2)}{\Gamma(\nu)} (1 + \|\xi\|_2^2)^{-(\nu + d/2)}.$$

Thus, the function $[\phi_0(c_2/(\phi q))]^{-1}$ has closed form as

$$\begin{aligned} [\phi_0(c_2/(\phi q))]^{-1} &= \frac{1}{\inf_{\|\xi\|_2 \leq 2c_2/q} \hat{K}_0(\xi)} \\ &= \frac{\Gamma(\nu) \{1 + 4c_2^2/(\phi^2 q^2)\}^{\nu + d/2}}{\tau^2 2^d \pi^{d/2} \Gamma(\nu + d/2)} = c_{m,1} \{1 + 4c_2^2/(\phi^2 q^2)\}^{\nu + d/2}, \end{aligned} \quad (\text{S23})$$

where $c_{m,1}$ is a constant dependent only on d, ν, τ^2 . Therefore, let $\rho = \frac{d^{1/2}}{\phi} \left[c_3 c_{m,1} \left(1 + \frac{4c_2^2}{\phi^2 q^2}\right)^{\nu + \frac{d}{2}} + \ln \left\{ c_{m,1} n q^{-d} \left(1 + \frac{4c_2^2}{\phi^2 q^2}\right)^{5(\nu + \frac{d}{2})} \right\} \right]^3$. We plug the results of equation (S23) and Technical Lemma S3 into equation (S22) to obtain that

$$\begin{aligned} W_2^2(Z_D, \hat{Z}_D) &\lesssim \frac{\exp \left[c_3 c_{m,1} \left(1 + \frac{c_2^2}{\phi^2 q^2}\right)^{\nu + \frac{d}{2}} + \ln \left\{ c_{m,1} n q^{-d} \left(1 + \frac{c_2^2}{\phi^2 q^2}\right)^{5(\nu + \frac{d}{2})} \right\} \right]}{\left(\exp \left[c_3 c_{m,1} \left(1 + \frac{c_2^2}{\phi^2 q^2}\right)^{\nu + \frac{d}{2}} + \ln \left\{ c_{m,1} n q^{-d} \left(1 + \frac{c_2^2}{\phi^2 q^2}\right)^{5(\nu + \frac{d}{2})} \right\} \right] \right)^3} \\ &= \frac{1}{\left(\exp \left[c_3 c_{m,1} \left(1 + \frac{c_2^2}{\phi^2 q^2}\right)^{\nu + \frac{d}{2}} + \ln \left\{ c_{m,1} n q^{-d} \left(1 + \frac{c_2^2}{\phi^2 q^2}\right)^{5(\nu + \frac{d}{2})} \right\} \right] \right)^2} \\ &= o(1) \end{aligned}$$

GAUSSIAN The Gaussian covariance function decays even faster than Matérn as the spatial distance increases. Therefore, we can let $r = 2$ and we have $Z \in \mathcal{Z}_{v_2}$ up to a scale parameter $a^{1/2}$. The Fourier transform of the d -dimensional Gaussian function K_0 under the case $a = 1$ is

$$\hat{K}_0(\xi) = \tau^2 \exp(-\|\xi\|_2^2/4).$$

Thus the function $\{\phi_0(c_2/(a^{1/2}q))\}^{-1}$ has the closed form solution as

$$\{\phi_0(c_2/(a^{1/2}q))\}^{-1} = \tau^{-2} \exp \left(\frac{c_2^2}{a q^2} \right). \quad (\text{S24})$$

Similar to the case of Matérn, we combine equation (S24) and equation (S22) to derive the condition on ρ as in Corollary 1.

GENERALIZED CAUCHY By definition, $K_0(\|s_1 - s_2\|_2) \lesssim 1/(1 + \|s_1 - s_2\|_2)^\lambda$. Thus $Z \in \mathcal{Z}_{c_r}$ and Theorem 2 can be directly applied here. By Theorem 1 of Bevilacqua and Faouzi (2019), we have

$$\{\phi_0(c_2 \phi / q)\}^{-1} \lesssim (2c_2 \phi / q)^{d+\delta},$$

where the multiplicative constant in the \lesssim relation only depends on $d, \tau^2, \lambda, \delta, \phi$. Therefore

$$\begin{aligned} W_2^2(Z_{\mathcal{D}}, \hat{Z}_{\mathcal{D}}) &\lesssim \frac{1}{(1 + \rho/(\phi d^{1/2}))^{\lambda-d-1}} nq^{(\lambda-8)d} (2c_2\phi/q)^{-(d+\delta)(\lambda+9/2)} (c_1c_5d2^{d-1}\pi/\sqrt{6})^\lambda \\ &\lesssim \frac{nq^{-d(\lambda+9/2+8-\lambda)-\delta(\lambda+9/2)}}{\{1 + \rho/(\phi d^{1/2})\}^{\lambda-d-1}} \\ &\lesssim \frac{nq^{-\frac{25}{2}d-\delta(\lambda+9/2)}}{\{1 + \rho/(\phi d^{1/2})\}^{\lambda-d-1}}. \end{aligned}$$

Setting the right-hand side to be $o(1)$ and reversely solving for ρ gives the condition on ρ in Corollary 1. \square

S4. POSTERIOR SAMPLING ALGORITHMS FOR RADGP REGRESSION

S4.1. Algorithm and Computational Complexity for Latent Effects Model

We provide the algorithm to perform the posterior sampling on the latent effects model described in Section 4 of the main paper.

Algorithm S1. Posterior Sampling for Latent RadGP Regression

Input training locations $\mathcal{T}_1 \subset \Omega$, test locations $\mathcal{T}_2 \subset \Omega$, covariates $X_{\mathcal{T}_1}, X_{\mathcal{T}_2}$ and response $Y_{\mathcal{T}_1}$.

Set an approximation radius ρ , the total number of MCMC steps l_1 and the number of burn-in steps l_2 ($l_2 < l_1$). Set initial values for β, θ, σ and $Z_{\mathcal{T}_1}$.

for $1 \leq l \leq l_1$ **do**

 Sample β from equation (12) in the main paper;

 Sample σ from equation (13) in the main paper;

 Generate random vector $W \sim N(\sigma^{-2}(Y_{\mathcal{T}_1} - X_{\mathcal{T}_1}\beta), \hat{\Phi} + I_n/\sigma^2)$ by

$W = \sigma^{-2}(Y_{\mathcal{T}_1} - X_{\mathcal{T}_1}\beta) + \hat{L}W_1 + \sigma^{-1}W_2$, where W_1, W_2 are independent

$N(0, I_n)$ random vectors and \hat{L} is the Cholesky factor of the precision matrix $\hat{\Phi}$;

 Compute a sample of $\hat{Z}_{\mathcal{T}_1}$ by solving the linear system $(\hat{\Phi} + I_n/\sigma^2)\hat{Z}_{\mathcal{T}_1} = W$, e.g., using conjugate gradient;

 Update θ using a Metropolis Hastings sampling step;

if $l \geq l_2$ **then**

 | Sample $\hat{Z}_{\mathcal{T}_2}$ according to equation (11).

Result: Output the posterior samples of $\beta, \theta, \delta, \hat{Z}_{\mathcal{T}_1}$ and $\hat{Z}_{\mathcal{T}_2}$.

We proceed to analyze the computational complexity of Algorithm S1. Since the number of MCMC steps l_1 is typical of order $10^3 \sim 10^5$, the cost of operations performed outside MCMC iterations (such as the construction of radial neighbors graph) is negligible. Hereafter we only analyze the operations inside the MCMC loop.

Recall that n denotes the sample size of training set \mathcal{T}_1 . Further let n_{test} be the sample size of test set, and d_β be the dimension of coefficients β . Sampling d_β from equation (12) in the main paper involves matrix inversion of dimension d_β and multiplication between $d_\beta \times n$ and $n \times d_\beta$ matrices, which takes $O(d_\beta^3 + nd_\beta^2)$ time. Once the mean and variance of β are computed, sampling β itself only takes $O(\beta)$ time. Assuming $d_\beta < n$, the time complexity of sampling β is $O(nd_\beta^2)$.

Sampling σ^2 from equation (13) in the main paper involves the computation of linear regression residuals for n training samples, which takes $O(n)$ time.

Next, we consider the computational complexity of sampling the spatial random effects $\hat{Z}_{\mathcal{T}_1}$ at the training locations. Let M_1 be the maximal number of parents in the radial neighbors graph on \mathcal{T}_1 . Computing the vector W involves the computation of Cholesky factor \hat{L} , which takes no more than $O(nM_1^3)$ time, and the matrix-vector multiplication between \hat{L} and W_1 , which takes $O(nM_1)$ time. The overall complexity of sampling W is no greater than $O(nM_1^3)$.

Let M_2 be the average number of nonzero elements per column in the precision matrix $\hat{\Phi}$. For RadGP, M_2 is equivalent to the number of locations within 2ρ radius, averaged at all training locations. If we solve the linear system $(\hat{\Phi} + I_n/\sigma^2)\hat{Z}_{\mathcal{T}_1} = W$ with conjugate gradients, the most costly operation in each iteration is the multiplication between the matrix $\hat{\Phi} + I_n/\sigma^2$ and a vector, which takes $O(nM_2)$ time. Let n_{cg} be the average number of conjugate gradient steps. In theory, n_{cg} can be as large as n ; in practice, under a fixed tolerance (10^{-6} in our package), n_{cg} can be much smaller than n . See Section S5.3 for some simulation studies. The total complexity of solving this linear system is $O(n_{cg}nM_2)$.

Let M_3 be the maximal number of parents in the radial neighbors graph on $\mathcal{T}_1 \cup \mathcal{T}_2$, the union of training and test sets. Sampling random effects on test locations is equivalent to sampling n_{test} unidimensional Gaussian distributions, which has the cost $O(n_{\text{test}}M_3^3)$.

Combining all the sampling steps, the overall time complexity of Algorithm S1 is

$$O(l_1n(d_\beta^2 + M_1^3 + n_{cg}M_2) + l_2n_{\text{test}}M_3^3). \quad (\text{S25})$$

In practice, n is usually much larger than M_1 , M_2 and M_3 to the point that M_i , $1 \leq i \leq 3$ can be regarded as constants compared to n . Assuming n_{test} is in the same order or smaller than n , then the most computationally expensive step is to sample the spatial random effects at the training locations because n_{cg} is the only variable (other than n itself) that increases with the sample size n . Therefore, the overall computational complexity in (S25) can be simplified to $O(M_2l_1nn_{cg})$.

If the spatial locations are distributed on a grid in \mathbb{R}^d with minimal separation distance q , then $M_2 \approx (\sqrt{\pi}\rho/q)^d \Gamma^{-1}(d/2 + 1)$. The overall computational complexity can be further simplified to $O(l_1nn_{cg}(\rho/q)^d)$. We can see the computational complexity is proportional to the d th power of approximation radius ρ , with smaller ρ leading to faster computation.

S4.2. Posterior Sampling for Response Model

Algorithm S1 outputs posterior samples of all spatial random effects along with posterior samples of parameters β, θ, δ . Because high dimensionality of the spatial random effects may negatively impact the mixing of MCMC chains, we directly approximate the marginal covariance using radial neighbors without estimating these latent effects. The resulting model of the response (Finley et al., 2019) only involves a low-dimensional parameter vector to be estimated via MCMC. Let $\tilde{Z}_{\mathcal{T}_1} = Z_{\mathcal{T}_1} + \epsilon_{\mathcal{T}_1}$ and $\tilde{Z}_{\mathcal{T}_2} = Z_{\mathcal{T}_2} + \epsilon_{\mathcal{T}_2}$. We use $\tilde{\Phi}$ to denote the RadGP precision that approximates $(\Sigma_{\mathcal{T}_1\mathcal{T}_1} + \sigma^2 I)^{-1}$. The joint posterior density now becomes

$$\det(\tilde{\Phi})^{1/2} \exp \left\{ -\frac{1}{2} (Y_{\mathcal{T}_1} - X_{\mathcal{T}_1}\beta)^T \tilde{\Phi} (Y_{\mathcal{T}_1} - X_{\mathcal{T}_1}\beta) \right\} p(\theta)p(\beta)p(\sigma^2),$$

where, using \hat{B} and \hat{D} as defined in Lemma S3, we have $\tilde{\Phi} = (I_n - \hat{B}^T)\hat{D}^{-1}(I_n - \hat{B})$, which is a sparse matrix. Let $\tilde{M} = \sup_{1 \leq i \leq n} |N(i)|$ be the maximal number of points in a radius ρ ball. By the derivation in Lemma S3, each row of \hat{B} has at most \tilde{M} nonzero elements, indicating that the computation of all rows of \hat{B} can proceed in parallel with a total computational com-

plexity $O(n\tilde{M}^3)$. Computations of the quadratic form $X_{\mathcal{D}}^T \tilde{\Phi} X$ and the determinant $\det(\tilde{\Phi})$ have $O(n\tilde{M}^2)$ and $O(n)$ time complexity, respectively.

Posterior sampling of unknown parameters proceeds as a hybrid Gibbs adaptive Metropolis-Hastings sampler. If the prior for β is normal, $\beta \sim N(\beta_0, \Phi_0^{-1})$, then the full conditional posterior distribution is also normal:

$$\beta | Y_{\mathcal{T}_1}, Z_{\mathcal{T}_1}, \sigma^2 \sim N((\Phi_0 + X_{\mathcal{T}_1}^T \tilde{\Phi} X_{\mathcal{T}_1})^{-1}(\Phi_0 \beta_0 + X_{\mathcal{T}_1}^T \tilde{\Phi} Y_{\mathcal{T}_1}), (\Phi_0 + X_{\mathcal{T}_1}^T \tilde{\Phi} X_{\mathcal{T}_1})^{-1}). \quad (\text{S26})$$

We use robust adaptive Metropolis-Hastings steps (Vihola, 2015) to update σ^2 and θ targeting an acceptance probability $\approx 24\%$. The sampling of $Y_{\mathcal{T}}$ given β, θ, σ^2 relies on:

$$\tilde{Z}_{\mathcal{T}_2} \sim N(\Sigma_{\mathcal{T}_2 \mathcal{T}_1} \hat{\Phi}(Y_{\mathcal{T}_1} - X_{\mathcal{T}_1} \beta), \Sigma_{\mathcal{T}_2 \mathcal{T}_2} - \Sigma_{\mathcal{T}_2 \mathcal{T}_1} \hat{\Phi} \Sigma_{\mathcal{T}_1 \mathcal{T}_2}), \quad (\text{S27})$$

$$\tilde{Y}_{\mathcal{T}_2} = X_{\mathcal{T}_2} \beta + \tilde{Z}_{\mathcal{T}_2}. \quad (\text{S28})$$

Algorithm S2 summarizes the MCMC for Bayesian inference of the RadGP response model.

Algorithm S2. Posterior Sampling for Response RadGP Process

Input training locations $\mathcal{T}_1 \subset \Omega$, test locations $\mathcal{T}_2 \subset \Omega$, covariates $X_{\mathcal{T}_1}$, $X_{\mathcal{T}_2}$ and response $Y_{\mathcal{T}_1}$.

Set an approximation radius ρ , iteration constants L_1, L_2 and initial values for β, θ, σ and $Z_{\mathcal{T}_1}$.

Compute the initial decomposition $\tilde{\Phi} = (I_n - \hat{B}^T) \hat{D}^{-1} (I_n - \hat{B})$.

for $1 \leq l \leq l_1$ **do**

 Sample β from equation (S26);

 Sample σ and θ from using Metropolis Hastings updates;

 Compute the decomposition $\tilde{\Phi} = (I_n - \hat{B}^T) \hat{D}^{-1} (I_n - \hat{B})$.

if $l \geq l_2$ **then**

 Sample $\tilde{Z}_{\mathcal{T}_2}$ according to equation (S27) and compute $\tilde{Y}_{\mathcal{T}_2}$ from equation (S28).

Result: Output the posterior samples of β, θ, δ and $\tilde{Z}_{\mathcal{T}_2}$.

Algorithm S2 does not require the computation of spatial random effects. Hence by a similar analysis for the latent effects model, the overall computational complexity is $O(l_1 n(d_\beta^2 + M_1^3) + l_2 n_{\text{test}} M_3^3)$.

S5. ADDITIONAL EXPERIMENTAL STUDIES

S5.1. Prior Approximations Under Increasing Domain Asymptotics

In this section, we employ an increasing domain asymptotic setting in a unidimensional space where the minimal separation distance is fixed at $q = 1/50$. As the sample size n increases, the size of domain Ω expands accordingly. We choose ρ as a function of n according to Corollary 1 and study how the prior approximation error changes as n increases. Specifically, we consider two covariance functions for the original Gaussian process: Matérn with smoothness $\nu = 3/2$ and generalized Cauchy with power $\lambda = 5$. Using the notations in Corollary 1, we choose parameters $(\phi, \tau^2, \nu) = (17.95, 1, 3/2)$ for Matérn and $(\phi, \tau^2, \lambda, \delta) = (2.13, 1, 5, 1)$ for generalized Cauchy. The ϕ parameter in both cases are chosen such that $K_0(0.15) = 0.25$. The approximation radius as a function of n is chosen to be $\rho(n) = (\log n)^3/200$ for Matérn and $\rho(n) = n^{1/2}/20$ for generalized Cauchy.

Because our main theorems only specify the upper bound of Wasserstein distance up to an absolute constant, it is necessary to numerically determine a “tight” constant. Specifically, for Matérn, we have set the theoretical upper bound to be $c_{\text{out}} n \exp(-c_{\text{in}} \rho)$. The constant c_{in} is selected so that $\exp(-c_{\text{in}} \rho)$ decays at about the same speed as the Matérn covariance function

in the domain of our simulation. The constant c_{out} is numerically adjusted to be the smallest constant such that the theoretical upper bound of the squared Wasserstein-2 distance W_2^2 is no smaller than simulated values for all n . This procedure yields $c_{in} = 13.68$ and $c_{out} = 5.19 \times 10^{-9}$. For the generalized Cauchy covariance function, we set the theoretical upper bound to be $c_{ca}n/(1 + \sqrt{n})^3$, where c_{ca} is determined numerically to be 7.71×10^{-3} .

The results for both simulated and theoretical upper bounds of W_2^2 are shown in Figure S1. We can see for both Matérn and generalized Cauchy covariance functions, the simulation curves decay at a faster rate compared to the theoretical upper bound. For the Matérn covariance function, the theoretical curve decays at a faster-than-polynomial but slower-than-exponential rate, whereas the simulation curve exhibits a roughly exponential decay. For the generalized Cauchy covariance function, the simulation curve initially increases when the sample size is small, and then it decreases faster than the theoretical curve as the sample size becomes large. These findings indicate that our current theoretical upper bounds may not be sufficiently tight. The actual decay rate of the Wasserstein-2 distance between the RadGP and the true Gaussian process could be faster than what we have proved in Corollary 1.

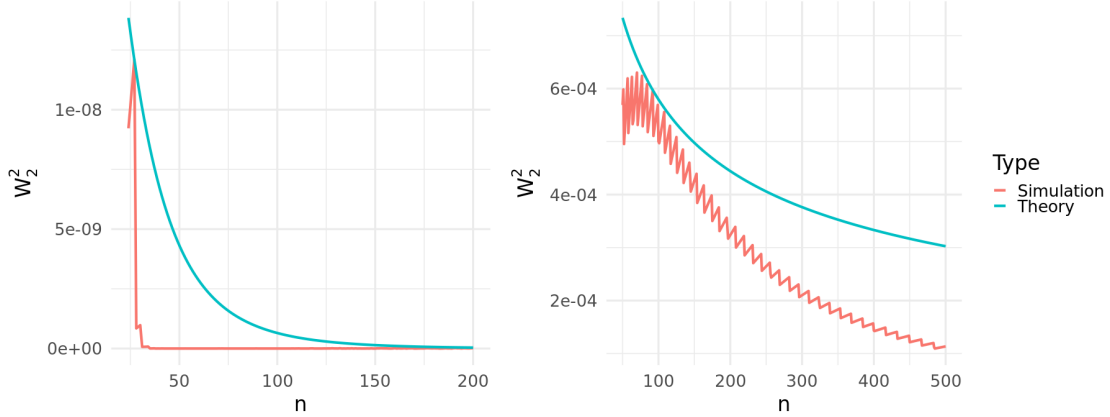


Fig. S1: Comparison between simulation and theoretical bounds under increasing domain asymptotics. X -axis is the sample size. Y -axis is the squared Wasserstein-2 distance. Left: Matérn covariance function with smoothness $\nu = 3/2$; Right: Generalized Cauchy covariance function with power $\lambda = 5$.

S5.2. Parameter Estimation

Recall that the Matérn covariance function is

$$K_0(x) = \frac{\tau^2 2^{1-\nu}}{\Gamma(\nu)} (\phi x)^\nu \mathcal{K}_\nu(\phi x).$$

In this section, we present the results of estimating the parameters ϕ , τ^2 and σ^2 under the same settings described in Section 5.2 of the main paper. The experiment is conducted once for each x -axis value, which represents the average number of nonzero elements per column in the precision matrix. We directly compute the posterior mean and 90% credible intervals for all parameters from the posterior samples. The results are shown in Figure S2. Generally, RadGP and NNGP exhibit similar performance in parameter estimation, with RadGP showing a slight advantage in estimating ϕ at large x -axis value. Neither method estimates τ^2 and the nugget σ^2 very effectively, which is not surprising as distinguishing the Gaussian process and the nugget effect is

known to be a difficult problem. According to the fixed domain asymptotic theory, when ϕ is known, the convergence rates of both frequentist estimators and Bayesian posteriors for τ^2 will deteriorate from a parametric rate in the model without nugget effect to a much slower nonparametric rate in the model with nugget effect (Chen et al., 2000; Tang et al., 2021; Li et al., 2023). The presence of the nugget effect means that increasing the complexity of graphical structure does not significantly improve the accuracy of parameter estimation.

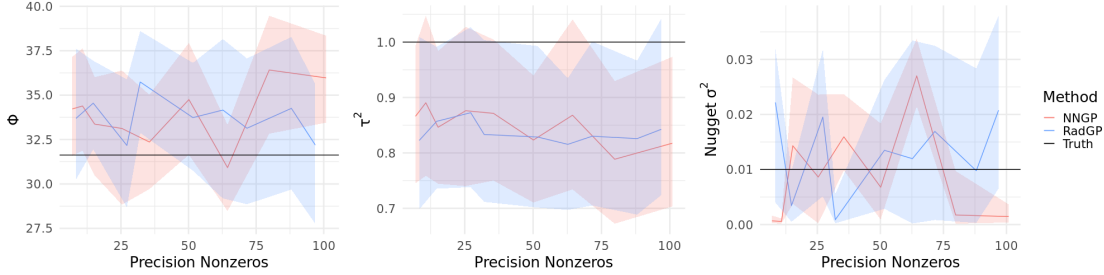


Fig. S2: Posterior mean and Bayesian credible intervals for parameters ϕ , τ^2 and σ^2 , where X -axis is the average number of nonzero elements per column in the precision matrix. Solid lines are the posterior means, and shaded regions are the 90% Bayesian credible intervals.

S5.3. MCMC Mixing and Conjugate Gradient Iterations

We study the posterior mixing of Algorithm S1 under the settings described in Section 5.2. Figure S3 displays the trace plots of the Gaussian process parameters ϕ , τ^2 and σ^2 for both RadGP and NNGP methods. The radius ρ for RadGP is set at 0.055, and the number of parents for NNGP is set at 4. With these parameter settings, the average number of nonzero elements per column in the precision matrix is 14.5 for RadGP and 15 for NNGP, which are very close.¹ We also plot the autocorrelation function for RadGP in Figure S4 (right). We omit the trace plots under other graph complexities and the autocorrelation plot for NNGP, as they are very similar to those displayed here.

Despite the requirement for MCMC to sample all spatial random effects, our simulation results suggest that the mixing for the Gaussian process parameters ϕ and τ^2 is quite good. The autocorrelation drops below 0.5 when the lag exceeds 7. Conversely, the posterior mixing for the nugget effect σ^2 is markedly slower. As discussed in Section S5.2, this phenomenon is attributed to the challenge of differentiating the nugget effect from the covariance function.

Figure S4 (left) displays the number of conjugate gradient iterations required under the settings described in Section 5.2. With a common tolerance of 10^{-6} , the average number of conjugate gradient iterations is approximately 7.5, with the 90% credible interval (2.6, 12.6), which is much smaller than the training sample size $n = 1600$.

S5.4. Prior and Posterior Approximations under Higher Spatial Correlation

In this section, we perform numerical studies for the case with denser training sets and high spatial correlations. Specifically, the training locations are set on a 50×50 equally spaced grid in $[0, 1]^2$. The length-scale parameter ϕ is selected so that $K(0.15) = 0.15$. The above configuration generates much stronger spatial dependence and 50% more training samples compared to the

¹ Because the locations are distributed on a grid and the number of parents for NNGP can only take integer numbers, the average number of nonzero elements can only take discrete values, making it impossible to set exactly the same average number of nonzeros for RadGP and NNGP methods.

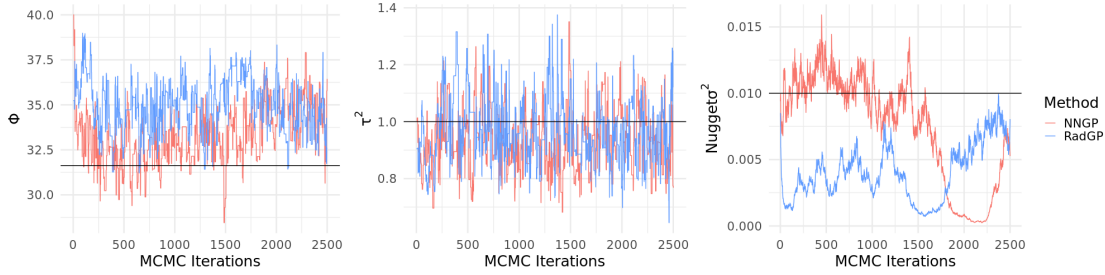


Fig. S3: Trace plots of model parameters ϕ , τ^2 and σ^2 for both RadGP and NNGP methods.

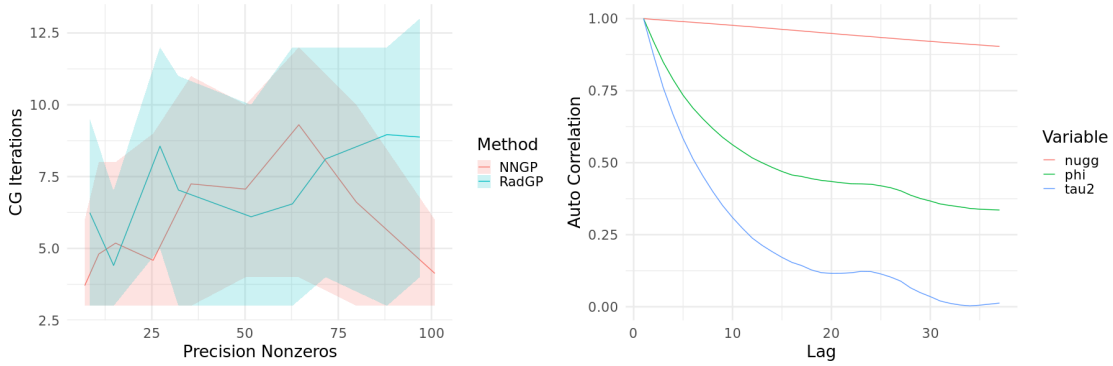


Fig. S4: Left: Number of conjugate gradient iterations under different graph complexities, where X -axis is the average number of nonzero elements per column in the precision matrix. Solid lines are the mean values and shaded regions are the 90% Bayesian credible intervals; Right: Autocorrelation functions for RadGP, where X -axis is the lag in the MCMC chains.

settings in Section 5.2. Other setups of the experiments are the same as described in Section 5.2. The prior and posterior comparisons are provided in Figures S5 and S6, respectively. For the prior comparison, we can see that RadGP performs better than NNGP when the average number of nonzero elements in the precision matrices is greater than 80. For the posterior comparison, while the Bayesian credible bands for all three methods largely overlap when the graph structure is sufficiently complex, RadGP outperforms the other two methods when the graph complexity is lower. Based on these comparisons, we conclude that RadGP performs at least as well as the state-of-the-art methods like NNGP in settings characterized by high spatial correlation.

S5.5. Prior and Posterior Approximations in 4-Dimensional Spaces

We examine the numerical performance of RadGP in the prior and posterior approximations with a 4-dimensional domain Ω . Due to the curse of dimensionality, setting the training locations on a regular grid is no longer feasible. Therefore, we draw 2500 training samples from a random Latin Hypercube design in $[0, 1]^4$ and fix them throughout the simulation studies in this section.² The posterior comparison consists of 50 repeated experiments. For each replication, the test data consist of another 2500 locations, complementing the training locations using random Latin hypercube design. The rest of the simulation settings are the same as described in Section 5.2.

² Changing training locations will also change the x -axis values (representing the average numbers of nonzeros in the precision matrix), which makes it harder to compare different methods. For simplicity, we fix the training locations. Based on our simulation studies, the key information conveyed by Figures S7 and S8 is insensitive to the randomness in training locations.

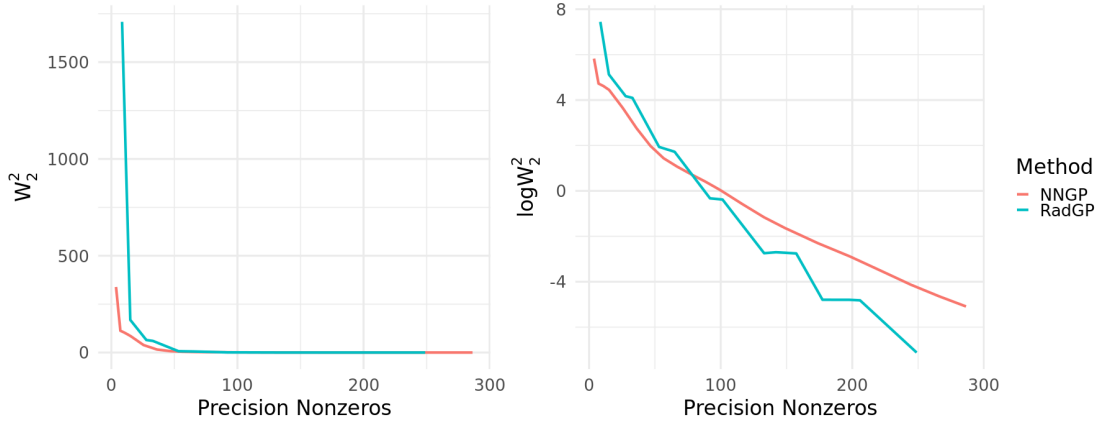


Fig. S5: Prior comparison for Matérn covariance function under the high spatial correlation setting. X-axis is the average number of nonzero elements per column in the precision matrix. Y-axis is the squared Wasserstein-2 distance and its logarithm.

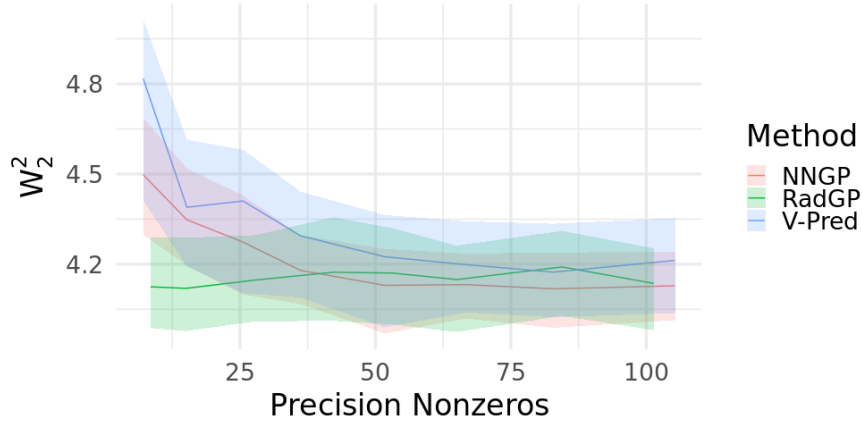


Fig. S6: Posterior comparison under the high spatial correlation setting. X-axis is the average number of nonzero elements per column in the precision matrix. Y-axis is the squared Wasserstein-2 distance. Solid lines are mean values and shaded regions are 90% Bayesian credible intervals.

The prior and posterior comparison are displayed in Figures S7 and S8. On the prior level, RadGP performs better than NNGP for the majority of x-axis values (the average numbers of nonzero elements in the precision matrix) considered in the comparison. However, all methods display equally large approximation errors for posterior prediction at the test locations, as measured in squared Wasserstein-2 distance. This indicates that the RadGP prior can still approximate the original Gaussian process prior accurately. However, due to the curse of dimensionality, all methods under investigation are unable to produce accurate posterior predictions of spatial random effects at unobserved locations with $n = 2500$ training samples in a 4-dimensional space.

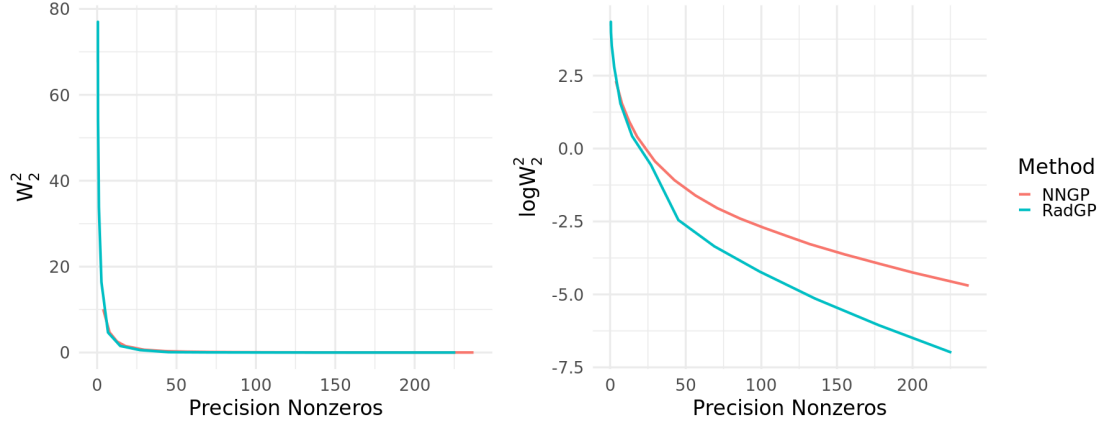


Fig. S7: Prior comparison for Matérn covariance function in a 4-dimensional space. X-axis is the average number of nonzero elements per column in the precision matrix. Y-axis is the squared Wasserstein-2 distance and its logarithm.

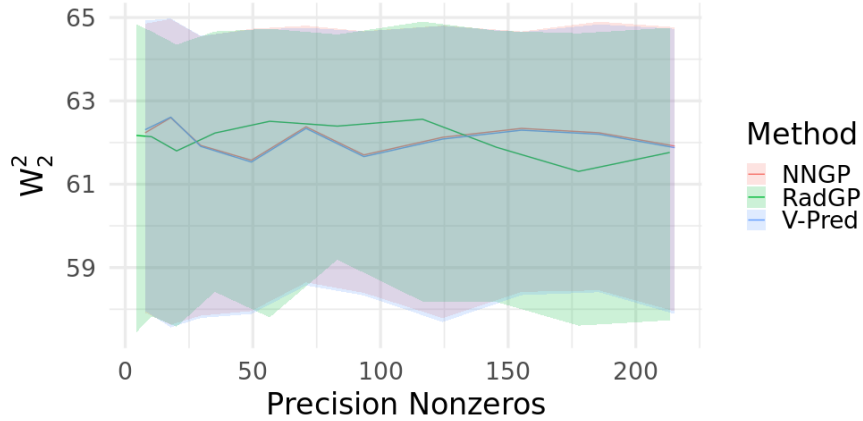


Fig. S8: Posterior comparison for Matérn covariance function in a 4-dimensional space. X-axis is the average number of nonzero elements per column in the precision matrix. Y-axis is the squared Wasserstein-2 distance. Solid lines are mean values and shaded regions are 90% Bayesian credible intervals.

S5.6. Discussion on NNGP and V-Pred

In the posterior comparison conducted in Section 5.2 of the main paper as well as Sections S5.4 and S5.5 above, NNGP performs similarly or sometimes even better than V-Pred in terms of the Wasserstein-2 distance between the posterior predictive distribution and the true predictive distribution. This phenomenon may appear confusing at first glance, since V-Pred allows dependence among the test locations and should ideally perform better. However, we must also take into account the impact of noise on prediction. In our numerical implementation, both V-Pred and NNGP have a fixed number of parents for all spatial locations. Therefore, compared to NNGP, for each test location, V-Pred will replace some parents in the training set with some parents in the test set that are closer. The presence of white noise makes the prediction of spatial

random effects on test locations not so good as that on training locations, which results in a worse prediction performance from V-Pred than NNGP on some occasions.

S6. DISCUSSION ON RADGP THEORY AND TAPERING-BASED GAUSSIAN PROCESSES THEORY

We would like to discuss the relations between our RadGP theory and the existing tapering-based Gaussian process theory (see for example, Furrer et al. 2006, Kaufman et al. 2008, Wang and Loh 2011, and Shaby and Ruppert 2012). Despite both theories working on the theoretical properties of Gaussian processes, these two theories exhibit the following four major differences.

First, the RadGP theory provided in this paper studies the finite sample approximation error bound of the radial neighbors Gaussian process, whereas the tapering-based Gaussian processes theory mainly studies the parameter estimation for the original Gaussian process. These two problems are different in the sense that an accurate finite sample approximation in Wasserstein distance does not imply good convergence rates in parameter estimation for the original process, and vice versa. To the best of our knowledge, we are not aware of any theory that provides the finite sample error bound for the approximation from either the covariance-tapered Gaussian processes or Vecchia approximated Gaussian processes to the original Gaussian processes in Wasserstein distance under either increasing domain or fixed domain asymptotics. Therefore, one major theoretical contribution in this paper is to introduce a new technique to spatial statistics, using the norm-controlled inversion of Banach algebras that can help quantify the approximation error for the radial neighbors Gaussian process. This new technique can potentially be further extended to other Vecchia approximation methods.

Second, the application scope of our RadGP theory and the previous tapering-based Gaussian processes theory are different. The theory of covariance tapering has mainly focused on parameter estimation for a parametric family of covariance functions, such as the isotropic Matérn covariance function, though in practice covariance tapering can be applied to any covariance function with good empirical performance for short range dependence. The setting of our RadGP theory is much more general and works for two large families of covariance functions ($\mathcal{L}_{v,r}$ and $\mathcal{L}_{c,r}$ defined in Equations (5) and (6) in the main paper) that only need to satisfy certain spatial decay conditions.

Third, since the Wasserstein-2 distance considered in our theory increases with the sample size (while decreases with the radius ρ), our current theorems and corollary work best for increasing domain and mixed domain asymptotics, but is not readily applicable to fixed domain (or infill) asymptotics. On the other hand, tapering-based Gaussian processes theory on parameter estimation, being well-developed in the literature, applies to both fixed domain asymptotics (Wang and Loh, 2011) and increasing domain asymptotics (Shaby and Ruppert, 2012).

Finally, besides the difference in theory, RadGP and covariance tapering are different Gaussian process methods. Covariance tapering multiplies the original covariance function by another covariance function that is identically zero outside of a specific range. As such, covariance tapering induces sparsity only in the spatial covariance matrix, but not in the precision matrix. In contrast, RadGP induces sparsity in the precision matrix, aiming to accelerate the evaluation of Gaussian likelihoods, similar to other Vecchia approximation methods.

REFERENCES

- Bevilacqua, M. and T. Faouzi (2019). Estimation and prediction of Gaussian processes using generalized Cauchy covariance model under fixed domain asymptotics. *Electronic Journal of Statistics* 13(2), 3025–3048.

- Chen, H.-S., D. G. Simpson, and Z. Ying (2000). Infill asymptotics for a stochastic process model with measurement error. *Statistica Sinica* 10, 141–156.
- Fang, Q. and C. E. Shin (2020). Norm-controlled inversion of Banach algebras of infinite matrices. *Comptes Rendus. Mathématique* 358(4), 407–414.
- Finley, A. O., A. Datta, B. D. Cook, D. C. Morton, H. E. Andersen, and S. Banerjee (2019). Efficient algorithms for Bayesian nearest neighbor Gaussian processes. *Journal of Computational and Graphical Statistics* 28(2), 401–414.
- Furrer, R., M. G. Genton, and D. Nychya (2006). Covariance tapering for interpolation of large spatial datasets. *Journal of Computational and Graphical Statistics* 15(3), 502–523.
- Gröchenig, K. and A. Klotz (2014). Norm-controlled inversion in smooth Banach algebras, II. *Mathematische Nachrichten* 287(8-9), 917–937.
- Kaufman, C. G., M. J. Schervish, and D. W. Nychka (2008). Covariance tapering for likelihood-based estimation in large spatial data sets. *Journal of the American Statistical Association* 103(484), 1545–1555.
- Li, C., S. Sun, and Y. Zhu (2023). Fixed-domain posterior contraction rates for spatial Gaussian process model with nugget. *Journal of the American Statistical Association* (forthcoming).
- Quang, M. H. (2023). Convergence and finite sample approximations of entropic regularized Wasserstein distances in Gaussian and RKHS settings. *Analysis and Applications* 21(3), 719–775.
- Shaby, B. and D. Ruppert (2012). Tapered covariance: Bayesian estimation and asymptotics. *Journal of Computational and Graphical Statistics* 21(2), 433–452.
- Tang, W., L. Zhang, and S. Banerjee (2021). On identifiability and consistency of the nugget in Gaussian spatial process models. *Journal of the Royal Statistical Society: Series B (Statistical Methodology)* 83(5), 1044–1070.
- Vihola, M. (2015). Robust adaptive Metropolis algorithm with coerced acceptance rate. *Statistics and Computing* 22, 997–1008.
- Wang, D. and W.-L. Loh (2011). On fixed-domain asymptotics and covariance tapering in Gaussian random field models. *Electronic Journal of Statistics* 5, 238–269.
- Wendland, H. (2004). *Scattered Data Approximation*, Volume 17. Cambridge University Press.